

ROBUST TRANSFER OF SAFETY-CONSTRAINED REINFORCEMENT LEARNING AGENTS

Anonymous authors

Paper under double-blind review

ABSTRACT

Reinforcement learning (RL) often relies on trial and error, which may cause undesirable outcomes. As a result, standard RL is inappropriate for safety-critical applications. To address this issue, one may train a safe agent in a controlled environment (where safety violations are allowed) and then transfer it to the real world (where safety violations may have disastrous consequences). Prior work has made this transfer safe as long as the new environment preserves the safety-related dynamics. However, in most practical applications, differences or shifts in dynamics between the two environments are inevitable, potentially leading to safety violations after the transfer. This work aims to guarantee safety even when the new environment has different (safety-related) dynamics. In other words, we aim to make the process of safe transfer robust. Our methodology (1) robustifies an agent in the controlled environment and (2) provably provides—under mild assumption—a safe transfer to new environments. The empirical evaluation shows that this method yields policies that are robust against changes in dynamics, demonstrating safety after transfer to a new environment.

1 INTRODUCTION

A prevalent strategy to render reinforcement learning (RL, Sutton & Barto, 2018) safe involves the use of transfer learning, where agents are initially trained in a controlled training environment, such as a simulation or a **laboratory** (Zhang et al., 2020). Since unsafe interactions with the controlled environment pose no real harm, these agents can be trained via standard safe reinforcement learning methods. The intention is to later transfer these trained agents to target environments where safety may be imperative (García & Fernández, 2015; Peng et al., 2021).

NEW

While numerous works have successfully maintained safety after transferring from a controlled training environment to the target (Yang et al., 2023; Feng et al., 2023; Gimelfarb et al., 2021; Karimpanal et al., 2020), their theoretical guarantees of safety rely on the strong assumption that safety-relevant dynamics remain unchanged between the two environments. However, the target environment likely differs from the training environment. Therefore, robustness to changes or shifts in dynamics plays a crucial role in realistic settings involving safety (Meng et al., 2023).

Problem statement. This work aims to train an agent in a controlled environment (where safety violations are allowed) to maintain safety throughout the process of transfer-learning, even under the worst-case transition dynamics in the new environment.

Taking inspiration from the method developed by Yang et al. (2023), we focus on a setting where an agent is trained within a reward-free environment, called the *source task* (\diamond). Here, the agent learns to navigate the environment safely *without* a reward signal. To account for potential differences in dynamics, we robustify this agent during the training in the source task by adding different kinds of action disturbances. These try to mimic changes in dynamics (different friction, mass, etc.) that would happen in an actual sim-to-real transfer setting, as these changes in dynamics can be viewed as additional disturbances in the system (Başar & Bernhard, 2008). More specifically, we use randomly sampled action noise (Hollenstein et al., 2022), adversarial action noise (Tessler et al., 2019), and entropy maximization (Ziebart et al., 2008; Eysenbach & Levine, 2022). Subsequently, this trained agent is transferred to a different environment, called the *target task* (\odot), where the

054
055
056
057
058
059
060
061
062
063
064
065
066
067
068
069
070
071
072
073
074
075
076
077
078
079
080
081
082
083
084
085
086
087
088
089
090
091
092
093
094
095
096
097
098
099
100
101
102
103
104
105
106
107

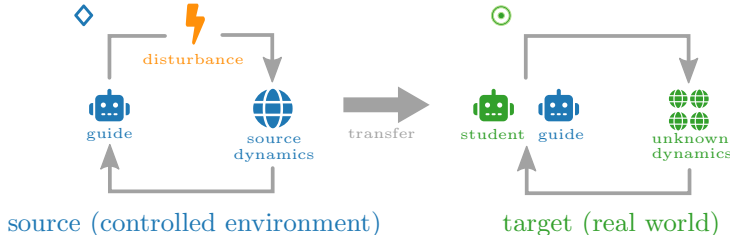


Figure 1: Training the guide under action disturbances in the source task and transferring it to teach the student in a target task with unknown dynamics.

reward is revealed. The trained agent, referred to as the *guide*, is then used to train a new agent, the *student*, while making sure that no safety-violations occur during training, as visualized in Figure 1.

Contributions. The key contributions of this paper are: 1. Introduce a mathematical framework for modeling robustness in the context of safe transfer learning. 2. Examine and compare how robustness during transfer is affected by entropy maximization, action noise, and adversarial action perturbations. 3. Propose an adaptation of an algorithm for safe transfer-learning developed by Yang et al. (2023) that accounts for uncertainties in the target environment. 4. Empirically and qualitatively analyze the proposed algorithm.

The empirical analysis shows that guides trained with action disturbances tend to have lower worst-case cumulative costs without compromising their overall performance. Furthermore, guides that are robust to changes in dynamics in the source task are better at transferring knowledge in challenging environments, with some achieving completely safe transfers, unlike non-robust ones.

2 RELATED WORK

Safety in RL. Traditionally, in RL, unsafe behavior is avoided through reward shaping by integrating the safety-related information into the reward signal (Laud & DeJong, 2003). However, such approaches demand significant engineering effort (Kamran et al., 2022; Roy et al., 2022). To avoid reward engineering, safety can be imposed through constraints (García & Fernández, 2015). The literature provides multiple types of constraints (Wachi et al., 2024). For instance, state-wise safety involves establishing state-specific hard constraints (Zhao et al., 2023; Zhan et al., 2023). Shielding is an example of a state-wise safe algorithm, where unsafe actions are blocked at runtime (Alshiekh et al., 2018; Carr et al., 2023). We focus on constraints in expectation, which allow a good trade-off between safety and performance (Altman et al., 2019).

Robust MDPs. Robustness is an essential component in sequential decision-making tasks when the transition function is unknown (Suilen et al., 2022; Cubuktepe et al., 2021; Moos et al., 2022). Robust constrained Markov decision processes (RCMDP) consider a set of potential transition dynamics, called *uncertainty set* (Russel et al., 2021). An agent is robustified in this framework by iteratively exposing it to the worst-case dynamics. Methods for solving RCMDPs involve computing the worst-case using linear programs (Russel et al., 2021), training an adversary to suggest such dynamics (Bossens, 2024), **applying perturbations to the transition function (Goyal & Grand-Clement, 2023)**, as well as combining homotopy continuation with bisection methods (Behzadian et al., 2021). **In contrast to the RCMDP framework, we assume that the uncertainty set is unknown during training, to reflect realistic scenarios. We aim to train agents that are capable of generalization to complete the task in an environment with newly revealed dynamics.**

NEW
NEW

Adversarial training. Adversarial training is a common method of achieving robustness (Moos et al., 2022). We may adversarially perturb observations by adding noise to sensors (Liu et al., 2023; Zhang et al., 2021), or the dynamics of the environment, for instance, by applying adversarial physical forces to the agent (Li et al., 2023). We adopt perturbations to the agent’s actions, as preliminary benchmarks showed that they consistently yielded the best results in our setting.

3 BACKGROUND

This section covers the theoretical foundations of our method.

Constrained Markov decision processes. A constrained Markov decision process (CMDP, Altman et al., 2019) is characterized by a tuple $\mathcal{M} = (S, A, P, r, c, d, \gamma)$, where S is the **continuous** state space, A is the **continuous** action space, $P: S \times A \rightarrow \text{Distr}(S)$ is the transition probability function with $\text{Distr}(S)$ being the set of probability measures on the Borel sets of S , $r: S \times A \rightarrow \mathbb{R}^+$ is the reward function, $c: S \times A \rightarrow \mathbb{R}^+$ is the cost function, $d \in \mathbb{R}^+$ is the cost-budget, and $\gamma \in [0, 1)$ is the discount factor. A *stationary stochastic policy* is a function $\pi: S \rightarrow \text{Distr}(A)$ that suggests a possibly stochastic action given the current state. We define the *set of stationary stochastic policies* as Π . The *expected cumulative reward* of policy π in state s over a finite horizon of length T is $V^\pi(s) = \mathbb{E}_\pi \left[\sum_{t=0}^T r(s_t, a_t) \gamma^t \mid s_0 = s \right]$, and the *expected cumulative cost* is defined similarly as $C^\pi(s) = \mathbb{E}_\pi \left[\sum_{t=0}^T c(s_t, a_t) \gamma^t \mid s_0 = s \right]$. The goal of the CMDP framework is to find an optimal policy π^* , that is, a policy that maximizes the expected cumulative reward while keeping the expected cumulative cost below d for all states $s \in S$:

$$\max_{\pi \in \Pi} V^\pi(s) \quad \text{s.t.} \quad C^\pi(s) \leq d.$$

The CMDP objective can be transformed with the Lagrangian relaxation method (Bertsekas, 1997),

$$\max_{\pi \in \Pi} \min_{\lambda \geq 0} V^\pi(s) - \lambda(C^\pi(s) - d).$$

We also define the *expected return* as $Q_\pi^r(s, a) = \mathbb{E}_\pi \left[\sum_{t=0}^T \gamma^t r(s_t, a_t) \mid s_0 = s, a_0 = a \right]$, and the *expected cost-return*, Q_π^c , is defined analogously.

Safe transfer-learning. In the transfer learning framework for RL, an agent must leverage the knowledge gained from the *source task* (\diamond) to learn the *target task* (\odot) more efficiently (Zhu et al., 2023). Said tasks are modeled by CMDPs in safety-critical applications, where the constraints model aspects concerning safety (García & Fernández, 2015; Peng et al., 2021). Yang et al. (2023) propose a reward-free source task $\mathcal{M}^\diamond = (S^\diamond, A^\diamond, P^\diamond, \emptyset, c^\diamond, d^\diamond, \gamma)$, where one can train an agent called the *guide*, with policy π^\diamond , that can safely navigate it without relying on a reward signal. This trained guide can then be used to train the *student* agent, with policy π^\odot , in the target task $\mathcal{M}^\odot = (S^\odot, A^\odot, P^\odot, r^\odot, c^\odot, d^\odot, \gamma)$.

Various transfer metrics exist for evaluating the extent to which one agent benefits from leveraging the knowledge of another agent (Taylor & Stone, 2009; Yang et al., 2023). One such metric is *safety jump-start*, which measures the difference in cumulative costs during the initial epoch between an agent that uses prior knowledge and one learning from scratch. Similarly, Δ *time to safety* assesses the difference in time required to reach safe behavior. Analogously, *return jump-start* and Δ *time to optimum* concern the reward signal.

4 ROBUST SAFE TRANSFER-LEARNING FRAMEWORK

This paper focuses on training a guide in the source task and transferring it to a target task that has different dynamics, which are unknown during the training of the guide, to then train a student while avoiding safety violations. Our source task is modeled by a reward-free CMDP $\mathcal{M}^\diamond = (S^\diamond, A^\diamond, P^\diamond, \emptyset, c^\diamond, d^\diamond, \gamma)$ as already introduced in the previous section. Since the dynamics of the target task are not known, we choose a more robust model. In particular, we model the target task as a CMDP where the transition function has been replaced by a *set of possible transition dynamics functions*, $\mathcal{M}^\odot = (S^\odot, A^\odot, U^\odot, r^\odot, c^\odot, d^\odot, \gamma)$, where every $P^\odot \in U^\odot$ is a dynamics function $P^\odot: S^\odot \times A^\odot \rightarrow \text{Distr}(S^\odot)$. We refer to U^\odot as the *uncertainty set*. One possible instance of such an uncertainty set is to define intervals of probabilities on transitions, creating infinitely many potential dynamics of the target task.

4.1 SAFETY GUARANTEES IN WORST-CASE ENVIRONMENTS

Since the intention is to transfer the policy of the guide, π^\diamond , from \mathcal{M}^\diamond to \mathcal{M}^\odot , both environments should share the same action space:

NEW
NEW
NEW

NEW

162 **Assumption 1.** $A^\diamond = A^\circ = A$.

163
164 Additionally, notice that the guide can only process observations from the source task’s state space
165 S^\diamond . Thus, to transfer the guide to the target task, we need to be able to map the state space of the
166 target task to the source space of the target task. In particular, we are interested in cases where this
167 mapping preserves information about the dynamics concerning safety to guarantee a safe transfer.
168 This concept is introduced by Li et al. (2006):

169 **Definition 1.** Function $\sigma: S \rightarrow S^\dagger$ is a Q^c -irrelevant abstraction for $\mathcal{M} = (S, A, P, r, c, d, \gamma)$
170 whenever $\forall s, s' \in S, \forall a \in A, \forall \pi \in \Pi, \sigma(s) = \sigma(s') \Rightarrow Q_{\pi, \mathcal{M}}^c(s, a) = Q_{\pi, \mathcal{M}}^c(s', a)$.

171
172 Similar model-invariant abstractions have been used in the CMDP setting to guarantee that safety
173 constraints are satisfied (Simão et al., 2021). Now, we assume that such a mapping exists from S°
174 to S^\diamond , and that this function **preserves boundedness**:

175 **Assumption 2.** There is a Q^c -irrelevant abstraction $\sigma: S^\circ \rightarrow S^\diamond$ for \mathcal{M}° that **preserves boundedness**.

176
177 Given an arbitrary Q^c -irrelevant abstraction, we consider how this function can map any CMDP \mathcal{M}
178 to a new CMDP \mathcal{M}^\dagger , the latter being referred to as the *abstracted task* (Li et al., 2006). **Refer to**
179 **Appendix C for an explicit construction**.

180 To clarify, even though σ maps the states in the target task to states in the source task, it does not
181 imply that the dynamics in the two tasks are similar, and it in fact does not concern the source task’s
182 dynamics in any manner. More precisely, Assumption 2 implies that the states in the target task can
183 be mapped to the states in the source task, where the information about the *target task’s dynamics* is
184 preserved, but the *source task’s dynamics* are not referenced and could thus be vastly different from
185 those of the target task.

186 Intuitively, σ strips away information that is not safety-relevant, to return a new abstracted CMDP
187 where the dynamics concerning safety are the same as in the initial CMDP. Therefore, one can
188 formally prove that an agent that is safe in the initial task is also safe in the abstracted task, as done
189 by Abel et al. (2016):

190 **Lemma 1.** Let $\sigma: S \rightarrow S^\dagger$ be Q^c -irrelevant, and tasks $\mathcal{M} = (S, A, P, r, c, d, \gamma)$ and
191 $\mathcal{M}^\dagger = (S^\dagger, A, P^\dagger, r^\dagger, c^\dagger, d, \gamma)$ constructed as in Appendix C. Then, $\forall s \in S, \forall a \in A, \forall \pi \in$
192 $\Pi^\dagger, Q_{\pi, \mathcal{M}^\dagger}^c(\sigma(s), a) = Q_{\pi \circ \sigma, \mathcal{M}}^c(s, a)$. \square

193
194 We have not yet imposed any restrictions on the uncertainty set, which means that the various dy-
195 namics transition functions in this set could potentially be infinitely different from each other. There-
196 fore, it is reasonable to disallow this by supposing that the uncertainty set is bounded:

197 **Assumption 3.** U° is bounded, that is, $\exists \varepsilon \in \mathbb{R}, \forall P, P' \in U^\circ, \|P - P'\| \leq \varepsilon$.

198
199 In the following theorem, we prove that an agent that is robust against changes in dynamics in the
200 source task will retain part of this robustness when transferred to the target task:

201 **Theorem 1.** Given Assumptions 1, 2, and 3, if $d^\diamond \leq d^\circ$ then there exists $\delta \in \mathbb{R}$ such that if policy
202 π is safe in \mathcal{M}_P^\diamond for all P where $\|P - P^\circ\| \leq \delta$, then $\pi \circ \sigma$ is safe in \mathcal{M}_P° for all $P' \in U^\circ$.

203
204 *Proof.* Since U° is bounded (Assumption 3) and σ preserves boundedness (Assumption 2), there is

$$205 \delta = \max_{P \in U^\circ} \|P^\dagger - P^\circ\|,$$

206
207 where the abstracted dynamics P^\dagger is constructed as in Appendix C. Now, suppose that π is safe for
208 all P with $\|P - P^\circ\| \leq \delta$, that is, $Q_{\pi, P}^{c, \diamond}(s, a) \leq d^\diamond$. Then, for all $P \in U^\circ$, we have $Q_{\pi, P^\dagger}^{c, \diamond}(s, a) \leq d^\diamond$
209 by construction of δ . Thus, $Q_{\pi \circ \sigma, P}^{c, \circ}(s, a) \leq d^\diamond \leq d^\circ$ given Lemma 1 and premise $d^\diamond \leq d^\circ$. \square

210
211
212
213
214 This proof is visualized in Figure 2. Theorem 1 justifies increasing δ in the source task with robust-
215 tification methods before transferring to a target task with uncertain dynamics, which is an essential
component in the method we introduce in Section 5.

216
217
218
219
220
221
222
223
224
225
226
227
228
229
230
231
232
233
234
235
236
237
238
239
240
241
242
243
244
245
246
247
248
249
250
251
252
253
254
255
256
257
258
259
260
261
262
263
264
265
266
267
268
269

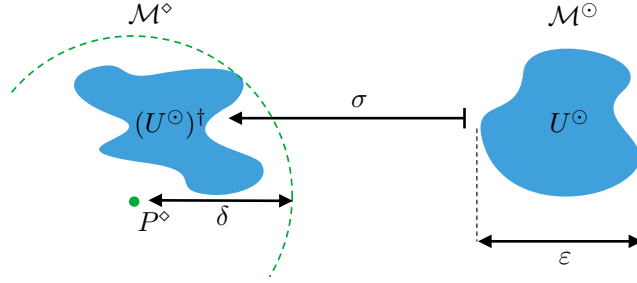


Figure 2: Visualization of the space of dynamics functions from Theorem 1.

4.2 ROBUST TRANSFER METRICS

Key insight. While an agent that is robust in the source task will also be robust in the target task, as shown in Theorem 1, this is not enough to be able to perform the transfer of knowledge successfully. To illustrate, notice that in many environments the “do nothing” policy is safe everywhere in U° , even though it is clear that this policy provides no value to train an agent in the target task. Thus, sometimes an agent that prioritizes exploration while taking more risks may be more useful for training another agent in the target task, compared to an overly conservative one, resulting in an overall lower cumulative cost. This serves as motivation for introducing metrics that measure the usefulness of the guide’s knowledge from the perspective of safety and robustness.

Let’s say that algorithm Φ uses the knowledge from the agent trained in the source task, π^\diamond , to train a new agent π° in the target task. To do so, the algorithm needs to sample K trajectories of length L in \mathcal{M}° , generating a history of environment interactions $\{\rho_i\}_{i=1,\dots,K}$. Since the algorithm may be nondeterministic, we have a history of probability distributions over the space of trajectories, denoted by $\rho_i \in \text{Distr}((S \times A)^* \times S)$ where the Kleene operator $(\cdot)^*$ indicates that we may have finite but arbitrarily long sequences of state and action pairs. This is expressed compactly as $\Phi(\pi^\diamond, \mathcal{M}^\circ) = \{\rho_i\}_{i=1,\dots,K}$, and we denote learning from scratch as $\Phi(\emptyset, \mathcal{M}^\circ)$.

NEW

Various transfer metrics exist for evaluating to which extent the target policy π° benefits from leveraging the knowledge of π^\diamond (Taylor & Stone, 2009), some of which have been adapted to account for safety by Yang et al. (2023). As these metrics have only been defined informally in prior work, we next provide rigorous definitions.

Definition 2. Given $\Phi(\pi^\diamond, \mathcal{M}^\circ) = \{\rho_i\}$ and $\Phi(\emptyset, \mathcal{M}^\circ) = \{\rho'_i\}$, the safety jump-start is defined as

$$\mathfrak{J}(\pi^\diamond, \mathcal{M}^\circ) = \mathbb{E} \left[\frac{c(\tau) - c(\tau')}{c(\tau')} \mid \tau \sim \rho_1, \tau' \sim \rho'_1 \right],$$

where $c((s_1, a_1, \dots, s_{L+1})) = \max(d^\circ, \sum_{i=1}^L \gamma^i c(s_i, a_i))$.

In other words, the safety jump-start measures the difference in excess cumulative costs during the initial trajectory or epoch between an agent that uses prior knowledge and one learning from scratch.

Definition 3. The Δ time to safety assesses the difference in time required to reach safe behavior. Given $\Phi(\pi^\diamond, \mathcal{M}^\circ) = \{\rho_i\}$ and $\Phi(\emptyset, \mathcal{M}^\circ) = \{\rho'_i\}$, the metric is defined as

$$\mathfrak{C}(P, \pi^\diamond) = \mathbb{E} [m(\{\tau'_i\}) - m(\{\tau_i\}) \mid \tau_i \sim \rho_i, \tau'_i \sim \rho'_i],$$

where $m(\{\tau_i\}) = \min_{t=1,\dots,L} t$ such that $\forall t' \geq t, c(\tau_{t'}) \leq d^\circ$.

Definition 4. Analogously to the safety jump-start and Δ time to safety, the return jump-start and Δ time to optimum concern the reward signal, respectively denoted by $\mathfrak{B}(\mathcal{M}^\circ, \pi^\diamond)$ and $\mathfrak{R}(\mathcal{M}^\circ, \pi^\diamond)$.

The transfer-learning problem at hand is to train the guide in a reward-free source task modeled by a CMDP, \mathcal{M}^\diamond , to later use it to learn a student policy in the target task modeled by a CMDP, \mathcal{M}° , with uncertainty set U° . It is important to bear in mind that \mathcal{M}° is completely inaccessible during the training of the guide in \mathcal{M}^\diamond , meaning that the guide cannot interact with U° during training.

Formal statement of the problem. Given a reward-free source CMDP \mathcal{M}^\diamond and a target CMDP \mathcal{M}° with uncertainty set U° , minimize the worst-case safety jump-start while keeping Δ time to

270 optimum above a threshold d_r :

$$271 \min_{\pi \in \Pi} \max_{P \in U^\circ} \mathfrak{J}(P, \pi) \text{ s.t. } \mathfrak{R}(P, \pi) \geq d_r.$$

272
273
274 Even though the problem statement only includes the safety jump-start and Δ time to optimum of
275 the guide, we are interested in measuring the Δ time to safety and return jump-start as well.

276 **Definition 5.** Given a policy $\pi \in \Pi$, the worst-case transition dynamics is

$$277 P^+ = \arg \max_{P \in U^\circ} \mathfrak{J}(P, \pi).$$

278 In practice, estimating the worst-case transition dynamics may require evaluating a policy within
279 various $P \in U^\circ$ and picking the environment that yields the highest cost. Consequently, notice
280 that we are likely to choose outliers through this process, causing the approximate worst-case safety
281 jump-start to have high variance. In an attempt to mitigate this issue, rather than selecting only one
282 environment, one can pick a portion $p \in [0, 1]$ of the environments where the agent performs the
283 worst. The following definition formalizes this concept.

284 **Definition 6.** For $p \in [0, 1]$, the p -tail of the safety jump-start is

$$285 \mathfrak{J}^{\leq p}(\mathcal{M}^\circ, \pi) = \int_B \mathfrak{J}(\mathcal{M}_P^\circ, \pi) dP,$$

286 if there exists $y \in \mathbb{R}$ such that $\frac{\|B\|}{\|U^\circ\|} = p$, where $B = \{P \in U^\circ \mid \mathfrak{J}(\mathcal{M}_P^\circ, \pi) \geq y\}$.

NEW

287
288 Additionally, $\mathfrak{J}^{\leq 1}(\mathcal{M}^\circ, \pi)$ is the average performance of π within the entirety of U° . While the
289 problem statement does not include the p -tail and average performance, we will keep track of them
290 in the empirical analysis.

291 5 ROBUST GUIDED SAFE EXPLORATION

292 Our method trains a robust guide via action disturbances in the source task and transfers it to the
293 target task to train the student safely.

294 5.1 TRAINING THE GUIDE

295 Since the source task is a reward-free CMDP, $\mathcal{M} = (S, A, P, \emptyset, c, d, \gamma)$, it is likely that an agent
296 trained in this environment would learn to “do nothing”, as it would only need to satisfy the safety
297 constraints. Therefore, we use a distance bonus to encourage the guide to explore the environment,

$$298 r^b(s_t, a_t) = \mathbb{E} \left[\|s_t^\ddagger - s_{t+1}^\ddagger\| \mid s_{t+1} \sim P(s_t, a_t) \right],$$

299 where $\|\cdot\|: S^\ddagger \rightarrow \mathbb{R}$ is a norm and $(\cdot)^\ddagger$ is a state abstraction function (Yang et al., 2023).

300 To transfer the guide to the uncertain target task, we must first robustify it during its training in the
301 source task. We employ three domain-agnostic robustification techniques.

302 **Entropy maximization.** To maximize the entropy of the agent, we include the following term in
303 the reward signal $r_t^\circ(s_t, a_t) = r_t^b(s_t, a_t) + \alpha r_t^{\mathcal{H}}(s_t, a_t)$, where $r_t^{\mathcal{H}}(s_t, a_t) = \log \frac{1}{\pi(a_t|s_t)}$.

304 **Random action noise.** Instead of sampling the action directly from the agent, some random noise
305 is added: $a \sim (1 - \alpha)\pi(s_t) + \alpha\mathcal{N}(\mu, \sigma)$.

306 **Adversarial perturbations.** The guide is trained in a noisy action robust MDP (Tessler et al.,
307 2019): $a \sim (1 - \alpha)\pi(s_t) + \alpha\bar{\pi}(s_t)$, where the guide is trying to maximize the objec-
308 tive $r_t^\circ = r_t^b$ while satisfying the cost constraints, and the adversary is trying to maximize
309 the cumulative cost.

310
311
312
313
314
315
316
317
318
319
320
321
322 Prior work has established that perturbation size (α) provably makes the policy robust to some
323 δ (Feng et al., 2020; Eysenbach & Levine, 2022). Therefore, as we increase the value of α , we are
effectively computing a robust policy for a larger uncertainty set in the source task. Consequently,

the agent will be safe in a larger set of target tasks. As a theoretical bound between α and δ can only be shown in specific scenarios, we adopt an empirical approach in the next section and evaluate the robustness effect across different values of α .

NEW

Note that Theorem 1 does not state that there always is a robustly safe policy. If δ is too large, such a policy may not exist. In practical terms, if we fail to find a feasible policy for a given δ , our method still attempts to find a conservative policy in the source target, which ensures a reduction of safety violations in the target environment. Alternatively, we could search for the largest $\delta' < \delta$ such that a feasible policy exists. Nevertheless, this policy can easily be found in the constrained RL setting. For instance, in problems exhibiting an action with zero cost, such as in the environments used in the empirical evaluation, the agent can choose this action, which ensures it will satisfy the constraints.

NEW

5.2 TRANSFERRING KNOWLEDGE TO THE STUDENT

To transfer the knowledge of the guide to the student, our approach is similar to (Yang et al., 2023). We want to ensure safety throughout by sampling from the student whenever the cost signal is zero, and otherwise we sample from the guide:

$$\pi^b(s_t) = \begin{cases} (\pi^\diamond \circ \sigma)(s_t) & \text{if there is a } t' \leq t \text{ where } c_{t'} > 0, \\ \pi^\circ(s_t) & \text{else.} \end{cases}$$

NEW

It is desirable to let the student’s policy imitate the guide’s whenever the cumulative cost is above the safety threshold, while this is not necessary once the student behaves safely. We achieve this effect by adding a new term r_t^\sim to the reward signal measuring the similarity between the two policies, weighted by the Lagrangian multiplier, λ . When both policies are nondeterministic, r_t^\sim measures the KL divergence between the two distributions. Otherwise, if either policy is deterministic, we compare the deterministic action with the mean of the nondeterministic policy’s distribution.

Reviewer LbED,
please notice that
we introduce λ
in Section 3.

6 EMPIRICAL ANALYSIS

We train one guide for each method of robustification (Section 5.1). Our empirical analysis aims to answer the following questions:

1. How does each guide perform in the source task?
2. How does each guide perform in the target task’s worst-case dynamics?
3. What is the safety jump-start of each guide in the target task?
4. How is the full training of the student affected by the guide’s robustness?

We evaluate **our method**¹ on benchmark environments created using a framework for safe reinforcement learning called *Safety-Gymnasium* (Ji et al., 2023). In these environments, the RL agent controls a robot that must reach the goal while avoiding the hazards. Appendix B provides more details.

NEW

The source tasks. There are three source tasks: (\mathcal{M}_1^\diamond , \mathcal{M}_2^\diamond , and \mathcal{M}_3^\diamond). These environments may contain static obstacles called *hazards* and dynamic obstacles called *vases*, which are always constrained. Additionally, all three environments have constrained walls to discourage the agent from going out of bounds. The environments differ as follows: \mathcal{M}_1^\diamond has 1 hazard located in the center; \mathcal{M}_2^\diamond has 5 hazards that change location every epoch, and \mathcal{M}_3^\diamond has 8 hazards and 8 vases that change location every epoch.

The target tasks. The target environments \mathcal{M}_1° , \mathcal{M}_2° , and \mathcal{M}_3° are similar to their respective source environments \mathcal{M}_1^\diamond , \mathcal{M}_2^\diamond , and \mathcal{M}_3^\diamond , except for two major differences.

1. The task in the target environments is to reach a specific location, called the *goal*. Therefore, the observations in the target tasks have the additional measurements that concern the

¹The source code is available on <https://anonymous.4open.science/r/KElzutXbe97jbuT>

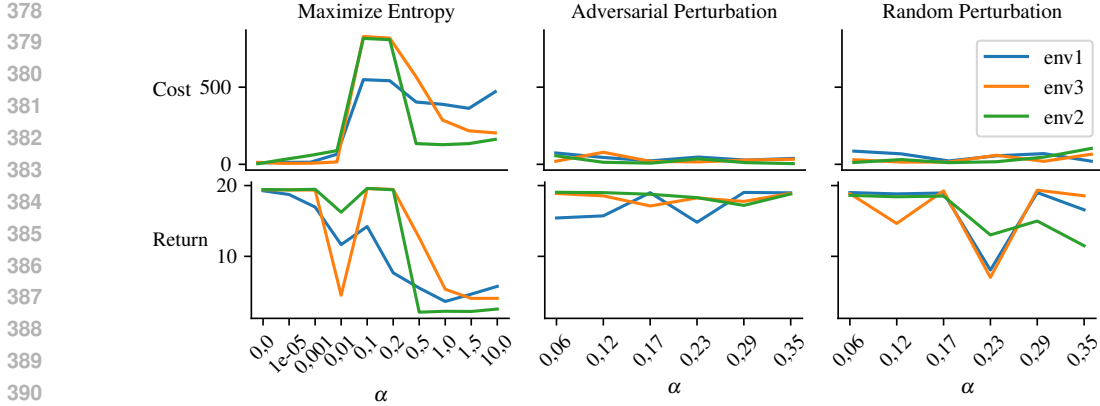


Figure 3: The cost and return in the last epoch of each type of guide.

reward signal: a LIDAR in $[0, 1]^{16}$ for detecting the goal. We have a mapping $\sigma: S^\odot \rightarrow S^\diamond$ which simply strips away the information concerning the reward signal. It is easy to show that σ is a Q^c irrelevance abstraction, satisfying Assumption 2.

- The transition dynamics function in the target tasks is uncertain. In our practical implementation, this is achieved by modifying the physics parameters concerning the *friction* and *mass* of the agent in the simulated environments. The friction refers to the force that opposes the motion of the robot, and a higher friction value causes the agent to decelerate quicker. The mass of the agent affects its moment of inertia, meaning that it impacts how quickly the agent can change its velocity.

One can define the function $u: \mathbb{R}^2 \rightarrow (S^\odot \times A \rightarrow \text{Distr}(S^\odot))$ that maps the friction and mass of the agent to the corresponding transition dynamics function. Thus, **notice that u preserves boundedness, which implies that U^\odot is bounded**, satisfying Assumption 3.

NEW

6.1 PERFORMANCE OF THE GUIDES IN THE SOURCE TASK

We train various guides with the three robustification techniques: random action noise, adversarial action perturbations, and entropy maximization. The guides are trained with different weights of the robustification methods to see which values of these parameters yield the best outcomes. The ranges of these weights are based on the results of prior work (Tessler et al., 2019; Liu et al., 2023): the random noise is weighted by $\alpha \in \{0.06, 0.12, 0.17, 0.23, 0.29, 0.35\}$; the adversarial perturbation weights are $\alpha \in \{0.06, 0.12, 0.17, 0.23, 0.29, 0.35\}$; and the entropy bonus is weighted by $\alpha \in \{10^{-5}, 10^{-3}, 10^{-2}, 0.1, 0.2, 0.5, 1.0, 1.5, 10.0\}$.

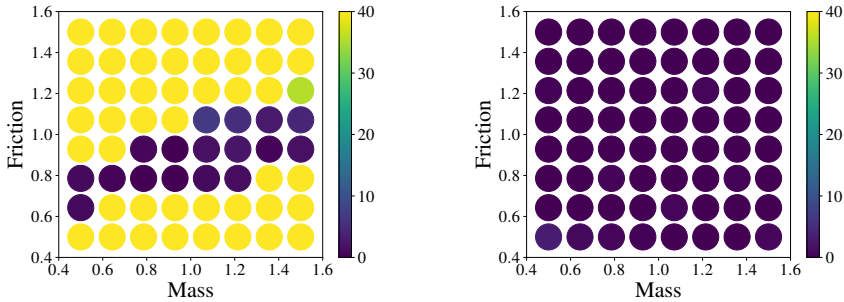
Figure 3 shows the cumulative returns and costs at the very last epoch of the three kinds of agents trained with the different values of the robustification weights. Most guides learn a safe policy that obtains a cumulative reward slightly below 20, except for the entropy-maximizing agent when $\alpha \geq 0.1$, which does not learn a proper policy, presumably due to the overly high entropy.

6.2 GUIDES’ PERFORMANCE IN THE TARGET TASK’S WORST-CASE DYNAMICS

The uncertainty set (U^\odot) consists of uncountably many dynamics transition functions, parameterized by the mass (m) and friction (η) of the agent, making it challenging to compute the worst-case dynamics. Therefore, we restrict the uncertainty set to a finite subset (\bar{U}^\odot) by discretizing the values of the parameters to $m = m_1, \dots, m_N$, and $\eta = \eta_1, \dots, \eta_N$. In our experiments, we use $N = 8$ values for each parameter by letting $m_i = (0.5 + \frac{i-1}{7})m^\diamond$ and $\eta_i = (0.5 + \frac{i-1}{7})\eta^\diamond$ for $i = 1, \dots, 8$, where m^\diamond and η^\diamond correspond to the dynamics in the source task.

First, we evaluate all guides within their respective source tasks, but instead of using the source task’s dynamics (P^\diamond), we evaluate them within the discretized uncertainty set of the target task, \bar{U}^\odot . This experiment provides insights into the relationship between the different robustification algorithms and the robustness they provide. Figure 4 shows the cumulative costs of a robust and non-robust agent evaluated in the dynamics functions of the discretized uncertainty set.

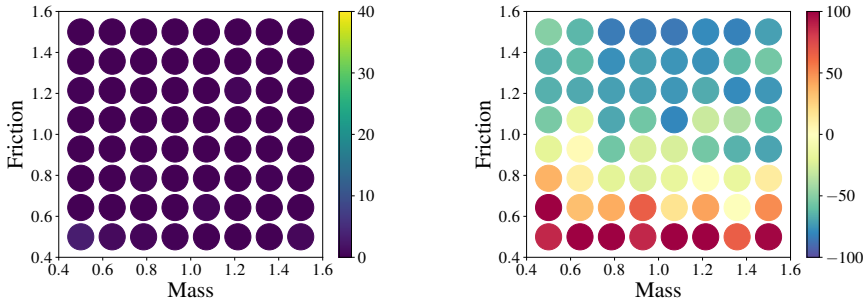
432
433
434
435
436
437
438
439
440
441



442
443
444
445

Figure 4: The expected cumulative costs in \mathcal{M}_1^\diamond of a guide trained with no action noise (left) and a guide with an action noise of $\alpha = 0.29$, each dot representing a different dynamics function, with mass on the x -axis and friction on the y -axis.

446
447
448
449
450
451
452
453
454
455
456



457
458
459
460

Figure 5: Expected cumulative cost in the source task (left) and the safety jump-start in the target task as a percentage (right) of the agent trained with $\alpha = 0.29$ within \mathcal{M}_1 . Low values of the safety jump-start are desirable, where a jump-start of -100 concerns a fully safe transfer.

461
462
463

The robust guide can navigate the source task safely even when the dynamics are unfavorable, while the non-robust agent struggles to maintain a safe expected cost when the shift in dynamics is large.

464
465
466
467
468
469
470
471
472

Heatmaps like the ones shown in Figure 4 have been computed for all three robustification methods and different values of α , and they can be seen in Appendix F. Once these heatmaps are calculated, it is easy to obtain the worst-case expected cost, as well as the p -tail and the average, shown in Tables 2, 3, and 4. It is crucial to note that the values shown in the tables are the expected costs of one batch of guides, implying that conclusions cannot be drawn from the comparison the values of α during training with their respective costs, due to a lack of statistical significance. Nevertheless, since the expected costs are computed quite accurately, it is correct to claim that some guides are more robust than others, which will be useful in the next sections to measure how the robustness of the guide impacts the student’s training in the target task.

473
474

6.3 SAFETY JUMP-START OF EACH GUIDE IN THE TARGET TASK’S WORST-CASE DYNAMICS

475
476
477
478
479

The safety jump-start assesses the difference in cumulative costs during the first epoch between the student learning from a guide and one learning from scratch. Measuring the safety jump-start is computationally cheap compared to other metrics, as it requires training the student for only one epoch as opposed to fully training said student.

480
481
482
483
484
485

We transfer the knowledge of the guides to two kinds of students: a nondeterministic student (SAC) and a deterministic one (DDPG). One major problem with transferring the knowledge to a deterministic student is that it is much likelier to end up in unrecoverable states by selecting the same actions over and over, rendering the control-switch rescue method completely ineffective. To lessen this issue, the deterministic student is trained with a relatively high random action noise of $\alpha = 0.75$.

Appendix G shows tables collecting the worst-case, 0.1-tail, and average safety jump-starts measured from every guide to the two kinds of students. An interesting observation when comparing

486
487
488
489
490
491
492
493
494
495
496
497
498
499
500
501
502
503
504
505
506
507
508
509
510
511
512
513
514
515
516
517
518
519
520
521
522
523
524
525
526
527
528
529
530
531
532
533
534
535
536
537
538
539

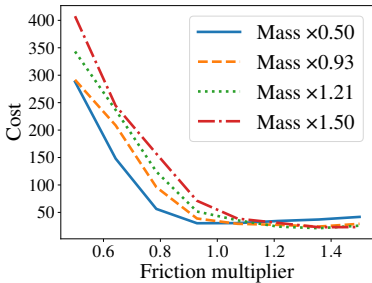


Figure 6: The expected cumulative costs in \mathcal{M}_2^\odot for the average guide given each mass-friction pair.

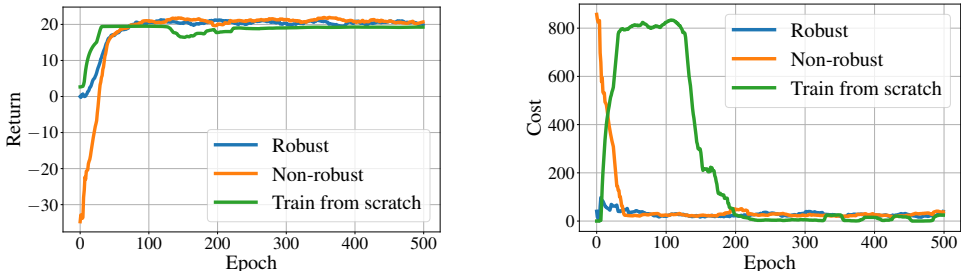


Figure 7: Comparison of the cumulative rewards and costs during training between the students trained with the robust guide ($\alpha = 0.29$) and the non-robust guide (Yang et al., 2023).

these with Tables 2, 3, and 4, is that policies that appear robust in the source task may not necessarily have the ability to effectively transfer their knowledge to a student in their target task. An extreme example of such a phenomenon can be seen in Figure 5, where an agent that is robust in the source task has an exceptionally poor safety jump-start in worst-case environments.

6.4 EFFECT OF THE GUIDE’S ROBUSTNESS ON THE STUDENT’S TRAINING

To determine how the transfer is affected by the robustness of the guide, we train the student with a robust guide and a non-robust one. For the robust guide, we will use the agent trained with action noise in \mathcal{M}_2 where $\alpha = 0.29$. **The non-robust guide is trained within \mathcal{M}_2 using the method introduced by Yang et al. (2023).** We then transfer the guides to the dynamics that appear most challenging based on the chart shown in Figure 6: $m^\odot = 1.5m^\diamond$ and $\eta^\odot = 0.5\eta^\diamond$.

NEW

The reward and cost during training of the students trained with robust and non-robust guides are shown in Figure 7. Since the goal of the transfer is to avoid safety violations within the target task, the transfer done with the robust guide seems ideal. Even though the training takes place in a task with unfavorable dynamics, the safety jump-start with the robust guide nears -100%, meaning that the behavior policy is safe from the very start. Moreover, the return jump-start of the student with the robust guide is much greater than that of the student with a non-robust guide.

7 CONCLUSIONS

We propose a method to transfer agents to environments with different or even worst-case dynamics while satisfying safety constraints. The empirical evaluation shows that, in general, agents trained with action disturbances have lower worst-case expected cumulative costs without sacrificing the expected return. In addition, we observe that guides that are robust in the source task do not always have a favorable worst-case jump-start, which backs our theoretical insights. Lastly, the agents with low worst-case safety jump-start demonstrate better capability for transferring knowledge to the student in unfavorable dynamics, compared to non-robust guides, where some robustified agents have been shown capable of achieving a fully safe transfer.

REFERENCES

- 540
541
542 David Abel, D. Ellis Hershkowitz, and Michael L. Littman. Near optimal behavior via approximate
543 state abstraction. In *ICML*, volume 48 of *JMLR Workshop and Conference Proceedings*, pp.
544 2915–2923. JMLR.org, 2016.
- 545 Mohammed Alshiekh, Roderick Bloem, Rüdiger Ehlers, Bettina Könighofer, Scott Niekum, and
546 Ufuk Topcu. Safe reinforcement learning via shielding. In *AAAI*, pp. 2669–2678. AAAI Press,
547 2018.
- 548
549 Eitan Altman, Said Boularouk, and Didier Josselin. Constrained Markov decision processes with
550 total expected cost criteria. In *VALUETOOLS*, pp. 191–192. ACM, 2019.
- 551 Tamer Başar and Pierre Bernhard. *H-infinity optimal control and related minimax design problems:
552 a dynamic game approach*. Springer Science & Business Media, 2008.
- 553
554 Bahram Behzadian, Marek Petrik, and Chin Pang Ho. Fast algorithms for l_∞ -constrained s-
555 rectangular robust mdps. In *NeurIPS*, pp. 25982–25992, 2021.
- 556 Dimitri P Bertsekas. Nonlinear programming. *Journal of the Operational Research Society*, 48(3):
557 334–334, 1997.
- 558
559 David M Bossens. Robust lagrangian and adversarial policy gradient for robust constrained Markov
560 decision processes. In *2024 IEEE Conference on Artificial Intelligence (CAI)*, pp. 1227–1239.
561 IEEE, 2024.
- 562 Steven Carr, Nils Jansen, Sebastian Junges, and Ufuk Topcu. Safe reinforcement learning via shield-
563 ing under partial observability. In *AAAI*, pp. 14748–14756. AAAI Press, 2023.
- 564
565 Murat Cubuktepe, Nils Jansen, Sebastian Junges, Ahmadreza Marandi, Marnix Suilen, and Ufuk
566 Topcu. Robust finite-state controllers for uncertain pomdps. In *AAAI*, pp. 11792–11800. AAAI
567 Press, 2021.
- 568
569 Benjamin Eysenbach and Sergey Levine. Maximum entropy RL (provably) solves some robust RL
570 problems. In *ICLR*. OpenReview.net, 2022.
- 571 Fei Feng, Ruosong Wang, Wotao Yin, Simon S. Du, and Lin F. Yang. Provably efficient exploration
572 for reinforcement learning using unsupervised learning. In *NeurIPS*, 2020.
- 573
574 Zeyu Feng, Bowen Zhang, Jianxin Bi, and Harold Soh. Safety-constrained policy transfer with
575 successor features. In *ICRA*, pp. 7219–7225. IEEE, 2023.
- 576
577 Javier García and Fernando Fernández. A comprehensive survey on safe reinforcement learning. *J.
578 Mach. Learn. Res.*, 16:1437–1480, 2015.
- 579 Michael Gimelfarb, André Barreto, Scott Sanner, and Chi-Guhn Lee. Risk-aware transfer in rein-
580 forcement learning using successor features. In *NeurIPS*, pp. 17298–17310, 2021.
- 581
582 Vineet Goyal and Julien Grand-Clement. Robust markov decision processes: Beyond rectangularity.
583 *Mathematics of Operations Research*, 48(1):203–226, 2023.
- 584 Jakob J. Hollenstein, Sayantan Auddy, Matteo Saveriano, Erwan Renaudo, and Justus H. Piater.
585 Action noise in off-policy deep reinforcement learning: Impact on exploration and performance.
586 *Trans. Mach. Learn. Res.*, 2022, 2022.
- 587
588 Jiaming Ji, Borong Zhang, Jiayi Zhou, Xuehai Pan, Weidong Huang, Ruiyang Sun, Yiran Geng,
589 Yifan Zhong, Juntao Dai, and Yaodong Yang. Safety-gymnasium: A unified safe reinforcement
590 learning benchmark, 2023.
- 591 Danial Kamran, Thiago D. Simão, Qisong Yang, Canmanie T. Ponnambalam, Johannes Fischer,
592 Matthijs T. J. Spaan, and Martin Lauer. A modern perspective on safe automated driving for
593 different traffic dynamics using constrained reinforcement learning. In *ITSC*, pp. 4017–4023.
IEEE, 2022.

- 594 Thommen George Karimpanal, Santu Rana, Sunil Gupta, Truyen Tran, and Svetha Venkatesh.
595 Learning transferable domain priors for safe exploration in reinforcement learning. In *IJCNN*,
596 pp. 1–10. IEEE, 2020.
- 597 Adam Laud and Gerald DeJong. The influence of reward on the speed of reinforcement learning:
598 An analysis of shaping. In *ICML*, pp. 440–447. AAAI Press, 2003.
- 600 Lihong Li, Thomas J. Walsh, and Michael L. Littman. Towards a unified theory of state abstraction
601 for MDPs. In *AI&M*, 2006.
- 602 Zeyang Li, Chuxiong Hu, Shengbo Eben Li, Jia Cheng, and Yunan Wang. Robust safe reinforcement
603 learning under adversarial disturbances. *CoRR*, abs/2310.07207, 2023.
- 605 Zuxin Liu, Zijian Guo, Zhepeng Cen, Huan Zhang, Jie Tan, Bo Li, and Ding Zhao. On the robust-
606 ness of safe reinforcement learning under observational perturbations. In *ICLR*. OpenReview.net,
607 2023.
- 608 Jinling Meng, Fei Zhu, Yangyang Ge, and Peiyao Zhao. Integrating safety constraints into adversar-
609 ial training for robust deep reinforcement learning. *Inf. Sci.*, 619:310–323, 2023.
- 611 Janosch Moos, Kay Hansel, Hany Abdulsamad, Svenja Stark, Debora Clever, and Jan Peters. Robust
612 reinforcement learning: A review of foundations and recent advances. *Mach. Learn. Knowl. Extr.*,
613 4(1):276–315, 2022.
- 614 Zhenghao Peng, Quanyi Li, Chunxiao Liu, and Bolei Zhou. Safe driving via expert guided policy
615 optimization. In *CoRL*, volume 164 of *Proceedings of Machine Learning Research*, pp. 1554–
616 1563. PMLR, 2021.
- 617 Julien Roy, Roger Girgis, Joshua Romoff, Pierre-Luc Bacon, and Christopher J. Pal. Direct behavior
618 specification via constrained reinforcement learning. In *ICML*, volume 162 of *Proceedings of*
619 *Machine Learning Research*, pp. 18828–18843. PMLR, 2022.
- 621 Reazul Hasan Russel, Mouhacine Benosman, Jeroen van Baar, and Radu Corcodel. Lyapunov robust
622 constrained-MDPs: Soft-constrained robustly stable policy optimization under model uncertainty.
623 *CoRR*, abs/2108.02701, 2021.
- 624 Thiago D. Simão, Nils Jansen, and Matthijs T. J. Spaan. Always safe: Reinforcement learning
625 without safety constraint violations during training. In *AAMAS*, pp. 1226–1235. ACM, 2021.
- 627 Marnix Suilen, Thiago D. Simão, David Parker, and Nils Jansen. Robust anytime learning of markov
628 decision processes. In *NeurIPS*, 2022.
- 629 R.S. Sutton and A.G. Barto. *Reinforcement Learning, second edition: An Introduction*. Adaptive
630 Computation and Machine Learning series. MIT Press, 2018. ISBN 9780262352703.
- 632 Matthew E. Taylor and Peter Stone. Transfer learning for reinforcement learning domains: A survey.
633 *J. Mach. Learn. Res.*, 10:1633–1685, 2009.
- 634 Chen Tessler, Yonathan Efroni, and Shie Mannor. Action robust reinforcement learning and applica-
635 tions in continuous control. In *ICML*, volume 97 of *Proceedings of Machine Learning Research*,
636 pp. 6215–6224. PMLR, 2019.
- 637 Akifumi Wachi, Xun Shen, and Yanan Sui. A survey of constraint formulations in safe reinforcement
638 learning. In Kate Larson (ed.), *Proceedings of the Thirty-Third International Joint Conference*
639 *on Artificial Intelligence, IJCAI-24*, pp. 8262–8271. International Joint Conferences on Artificial
640 Intelligence Organization, 8 2024. doi: 10.24963/ijcai.2024/913. URL [https://doi.org/](https://doi.org/10.24963/ijcai.2024/913)
641 [10.24963/ijcai.2024/913](https://doi.org/10.24963/ijcai.2024/913). Survey Track.
- 642 Qisong Yang, Thiago D. Simão, Nils Jansen, Simon H. Tindemans, and Matthijs T. J. Spaan. Re-
643 inforcement learning by guided safe exploration. In *ECAI*, volume 372 of *Frontiers in Artificial*
644 *Intelligence and Applications*, pp. 2858–2865. IOS Press, 2023.
- 645 Simon Sinong Zhan, Yixuan Wang, Qingyuan Wu, Ruochen Jiao, Chao Huang, and Qi Zhu. State-
646 wise safe reinforcement learning with pixel observations. *CoRR*, abs/2311.02227, 2023.

648 Huan Zhang, Hongge Chen, Duane S. Boning, and Cho-Jui Hsieh. Robust reinforcement learning
649 on state observations with learned optimal adversary. In *ICLR*. OpenReview.net, 2021.
650

651 Jesse Zhang, Brian Cheung, Chelsea Finn, Sergey Levine, and Dinesh Jayaraman. Cautious adap-
652 tation for reinforcement learning in safety-critical settings. In *ICML*, volume 119 of *Proceedings*
653 *of Machine Learning Research*, pp. 11055–11065. PMLR, 2020.

654 Weiye Zhao, Tairan He, Rui Chen, Tianhao Wei, and Changliu Liu. State-wise safe reinforcement
655 learning: A survey. In *IJCAI*, pp. 6814–6822. ijcai.org, 2023.
656

657 Zhuangdi Zhu, Kaixiang Lin, Anil K. Jain, and Jiayu Zhou. Transfer learning in deep reinforcement
658 learning: A survey. *IEEE Trans. Pattern Anal. Mach. Intell.*, 45(11):13344–13362, 2023.

659 Brian D. Ziebart, Andrew L. Maas, J. Andrew Bagnell, and Anind K. Dey. Maximum entropy
660 inverse reinforcement learning. In *AAAI*, pp. 1433–1438. AAAI Press, 2008.
661
662
663
664
665
666
667
668
669
670
671
672
673
674
675
676
677
678
679
680
681
682
683
684
685
686
687
688
689
690
691
692
693
694
695
696
697
698
699
700
701

A HYPERPARAMETERS

The hyperparameters in our method are summarized in Table 1. All actor and critic networks are modeled by a multilayer perceptron (MLP).

Parameter	\mathcal{M}_1	\mathcal{M}_2	\mathcal{M}_3
Actor network size	[256, 256]	[256, 256]	[256, 256]
Critic network size	[256, 256]	[256, 256]	[256, 256]
Size of replay buffer	10^6	10^6	10^6
Batch size	256	256	256
Steps per epoch	2000	2000	2000
Number of epochs	10^6	10^6	10^6
Actor learning rate	$5 \cdot 10^{-6}$	$5 \cdot 10^{-6}$	$5 \cdot 10^{-6}$
Critic learning rate	10^{-3}	10^{-3}	10^{-3}
Lambda learning rate	$5 \cdot 10^{-7}$	$5 \cdot 10^{-7}$	$5 \cdot 10^{-7}$
Safety constraint	5	8	25

Table 1: The hyperparameters used in the experiments.

B THE ENVIRONMENTS

The actor is a small robot called the *point* that can move forwards, backwards, and steer left-to-right. The action space is $[-1, 1]^2$, where the first value is for the throttle and the second one is for steering. The observation space has the following components:

- Pseudo-LIDAR for hazards in $[0, 1]^{16}$.
- Pseudo-LIDAR for vases in $[0, 1]^{16}$.
- Velocimeter in $(-\infty, \infty)^3$.
- Accelerometer in $(-\infty, \infty)^3$.
- Gyroscope in $(-\infty, \infty)^3$.
- Magnetometer in $(-\infty, \infty)^3$.

The pseudo-LIDAR casts 16 rays in different angles. It is termed “pseudo” because, unlike with real LIDARs, the rays can go through objects. The other sensors measure in three dimensions: a velocimeter for velocity (m/s), an accelerometer for acceleration (m/s²), a gyroscope for angular velocity (rad/s), and a magnetometer for magnetic flux (Wb).

Renders of the tasks are shown in Figures 8, 9, and 10.

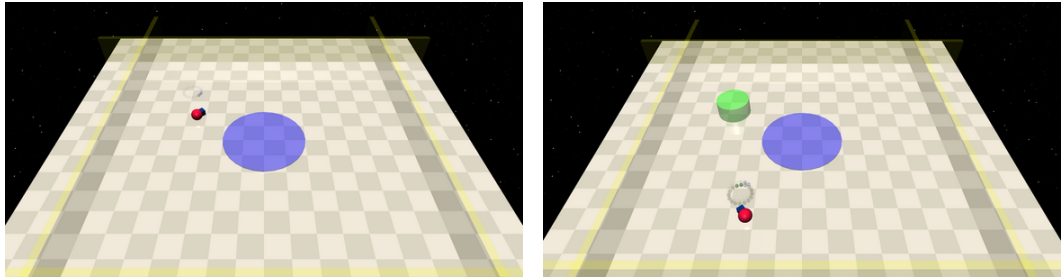


Figure 8: Renders of tasks \mathcal{M}_1° (left) and \mathcal{M}_1^\ominus (right).

756
757
758
759
760
761
762
763
764
765
766
767
768
769
770
771
772
773
774
775
776
777
778
779
780
781
782
783
784
785
786
787
788
789
790
791
792
793
794
795
796
797
798
799
800
801
802
803
804
805
806
807
808
809

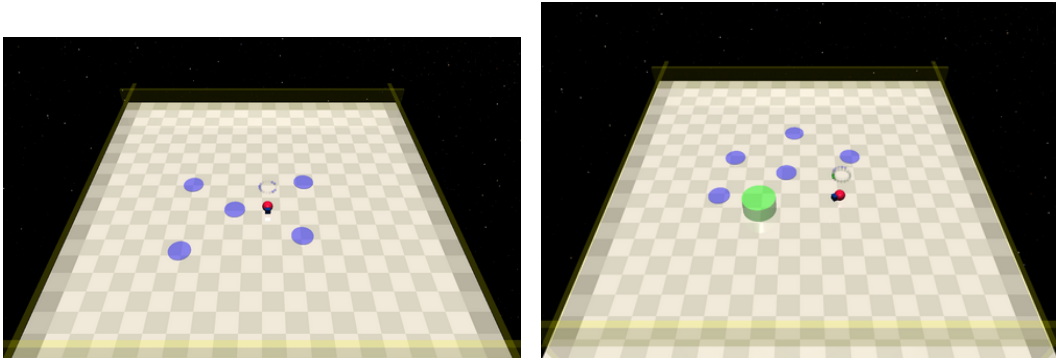


Figure 9: Renders of tasks \mathcal{M}_2° (left) and \mathcal{M}_2^{\odot} (right).

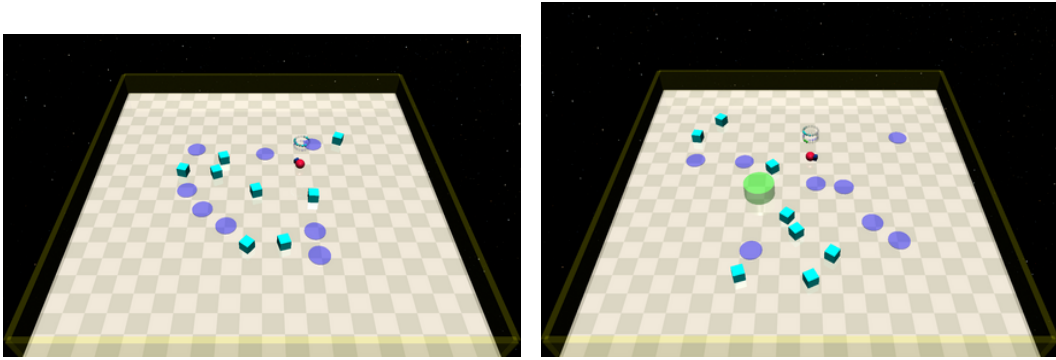


Figure 10: Renders of tasks \mathcal{M}_3° (left) and \mathcal{M}_3^{\odot} (right).

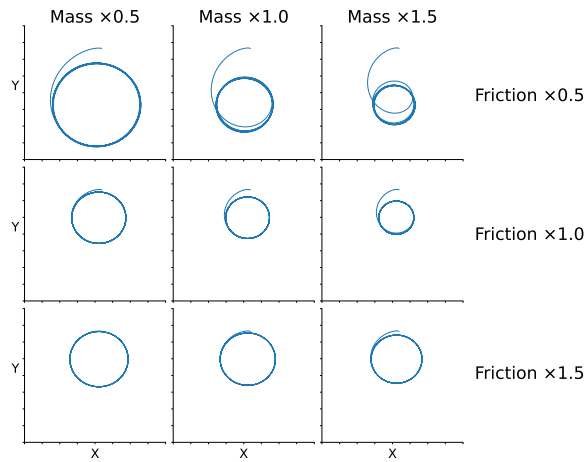


Figure 11: The trajectories of $\pi(\cdot) = (1.0, 1.0)$ where the mass and damping are multiplied by 0.5, 1.0, and 1.5. Both multipliers are 1.0 in the nominal dynamics.

C STATE ABSTRACTION

A Q^c -irrelevant abstraction $\sigma: S \rightarrow S^\dagger$ maps a CMDP to an *abstracted* CMDP (Li et al., 2006). Let $\mathcal{M} = (S, A, P, r, c, d, \gamma)$, and $\omega: S \rightarrow [0, 1]$. The corresponding *abstracted task* is $\mathcal{M}^\dagger = (S^\dagger, A, P^\dagger, r^\dagger, c^\dagger, d, \gamma)$, where

NEW

- $P^\dagger(s'^\dagger | s^\dagger, a) = \sum_{s \in \sigma^{-1}(s^\dagger)} \sum_{s' \in \sigma^{-1}(s'^\dagger)} \omega(s) P(s' | s, a)$,
- $r^\dagger(s^\dagger, a) = \sum_{s \in \sigma^{-1}(s^\dagger)} \omega(s) r(s, a)$,
- $c^\dagger(s^\dagger, a) = \sum_{s \in \sigma^{-1}(s^\dagger)} \omega(s) c(s, a)$,

with $\sigma^{-1}(s^\dagger) = \{s \in S \mid \sigma(s) = s^\dagger\}$ and $\sum_{s \in \sigma^{-1}(s^\dagger)} \omega(s) = 1$, for all $s^\dagger \in S^\dagger$.

D CUMULATIVE COSTS IN THE UNCERTAINTY SETS

α	\mathcal{M}_1^\diamond			\mathcal{M}_2^\diamond			\mathcal{M}_3^\diamond		
	Worst	0.1-tail	Avg.	Worst	0.1-tail	Avg.	Worst	0.1-tail	Avg.
0.00	805.1	780.2	316.7	862.6	856.2	268.6	536.9	457.9	89.3
0.06	843.2	816.6	221.5	353.3	221.4	41.2	635.0	574.5	130.6
0.12	873.5	868.2	438.1	842.8	792.9	179.2	89.7	77.2	34.2
0.17	780.8	683.9	150.5	692.8	399.0	110.4	725.0	569.0	95.8
0.23	2.3	1.5	0.2	91.3	77.7	21.5	286.2	268.8	126.5
0.29	3.2	1.1	0.1	95.7	59.7	18.1	859.0	754.0	168.2
0.35	134.5	100.0	11.5	271.6	162.9	58.6	833.6	809.0	190.1

Table 2: The worst-case, 0.1-tail, and average expected costs of all the guides trained with *random action noise* within the three source tasks.

α	\mathcal{M}_1^\diamond			\mathcal{M}_2^\diamond			\mathcal{M}_3^\diamond		
	Worst	0.1-tail	Avg.	Worst	0.1-tail	Avg.	Worst	0.1-tail	Avg.
0.0	805.1	780.2	316.7	862.6	856.2	268.6	536.9	457.9	89.3
0.06	880.4	871.5	537.2	769.5	717.3	108.6	219.7	210.3	49.0
0.12	840.0	821.7	302.7	626.6	569.8	75.8	338.1	218.5	45.3
0.17	484.0	367.2	87.7	713.9	554.1	109.7	166.4	148.3	65.5
0.23	790.7	774.8	372.5	773.0	678.9	97.5	459.9	335.5	102.8
0.29	38.5	17.5	2.7	233.8	212.4	52.6	699.5	640.5	143.7
0.35	742.5	687.9	294.2	211.4	139.0	57.2	255.3	225.7	84.7

Table 3: The worst-case, 0.1-tail, and average expected costs of all the guides trained with *adversarial perturbations* within the three source tasks.

α	\mathcal{M}_1^\diamond			\mathcal{M}_2^\diamond			\mathcal{M}_3^\diamond		
	Worst	0.1-tail	Avg.	Worst	0.1-tail	Avg.	Worst	0.1-tail	Avg.
0.0	147.4	82.9	9.7	668.7	563.6	108.2	892.7	881.7	262.4
10^{-3}	594.2	139.0	13.2	551.1	423.1	59.3	877.6	871.0	186.4

Table 4: The worst-case, 0.1-tail, and average expected costs of all the guides trained with *entropy maximization* within the three source tasks.

E SAFETY JUMP-START TABLES

α	\mathcal{M}_1^\diamond			\mathcal{M}_2^\diamond			\mathcal{M}_3^\diamond		
	Worst	0.1-tail	Avg.	Worst	0.1-tail	Avg.	Worst	0.1-tail	Avg.
0.06	-60.4	-62.1	-86.6	-56.3	-63.0	-87.4	-48.9	-55.1	-82.9
0.12	-49.6	-54.3	-80.9	-31.4	-39.2	-84.1	-41.5	-53.6	-80.2
0.17	-64.3	-69.8	-87.9	-32.4	-51.2	-83.9	-36.6	-47.6	-80.8
0.23	-71.2	-80.3	-91.9	-34.8	-49.7	-85.2	-23.7	-39.1	-75.0
0.29	-62.8	-65.2	-86.5	-55.8	-59.5	-87.3	-15.6	-25.7	-76.4
0.35	-49.3	-61.8	-87.5	-5.8	-35.7	-79.6	-29.7	-38.6	-78.9

Table 5: *Deterministic students with the random action noise guide.*

α	\mathcal{M}_1^\diamond			\mathcal{M}_2^\diamond			\mathcal{M}_3^\diamond		
	Worst	0.1-tail	Avg.	Worst	0.1-tail	Avg.	Worst	0.1-tail	Avg.
0.06	179.7	134.9	-17.6	50.6	13.1	-63.0	18.8	2.7	-57.9
0.12	263.5	183.3	15.9	138.2	105.3	-47.3	64.5	40.4	-50.6
0.17	156.9	101.6	-20.3	123.1	53.2	-51.3	70.1	29.1	-53.1
0.23	46.7	18.7	-52.3	117.4	47.8	-56.1	68.5	48.0	-47.0
0.29	195.0	126.4	-18.8	86.2	26.8	-63.7	126.7	105.7	-41.1
0.35	205.1	103.8	-28.7	135.2	92.8	-41.1	116.2	63.2	-51.6

Table 6: *Nondeterministic students with the random action noise guide.*

α	\mathcal{M}_1^\diamond			\mathcal{M}_2^\diamond			\mathcal{M}_3^\diamond		
	Worst	0.1-tail	Avg.	Worst	0.1-tail	Avg.	Worst	0.1-tail	Avg.
0.06	-50.8	-57.0	-82.7	-44.9	-52.4	-84.1	-41.7	-49.0	-79.8
0.12	-56.6	-63.0	-87.2	-31.3	-39.9	-83.2	-39.7	-51.2	-81.3
0.17	-68.4	-72.1	-88.6	17.3	-28.9	-78.8	-41.8	-52.4	-80.8
0.23	-52.7	-64.4	-85.7	-19.9	-29.9	-80.5	-49.7	-58.6	-83.2
0.29	-62.0	-69.4	-87.8	-31.8	-49.4	-83.5	-52.3	-59.1	-82.9
0.35	-65.0	-67.6	-80.5	-61.0	-68.2	-88.4	-48.8	-52.4	-79.9

Table 7: *Deterministic students with the adversarially trained guide.*

α	\mathcal{M}_1^\diamond			\mathcal{M}_2^\diamond			\mathcal{M}_3^\diamond		
	Worst	0.1-tail	Avg.	Worst	0.1-tail	Avg.	Worst	0.1-tail	Avg.
0.06	177.7	143.1	0.2	151.5	86.9	-50.1	61.7	30.8	-52.5
0.12	106.3	88.9	-30.8	142.1	102.6	-46.3	43.0	25.6	-54.8
0.17	73.6	53.4	-36.2	161.0	122.9	-36.3	21.2	13.4	-54.3
0.23	197.2	125.7	-14.2	135.2	99.9	-44.9	40.9	21.3	-55.6
0.29	188.7	101.0	-23.7	86.6	36.1	-55.4	24.1	1.3	-59.4
0.35	172.2	112.2	10.1	56.3	26.5	-63.5	74.1	39.4	-50.2

Table 8: *Nondeterministic students with the adversarially trained guide.*

α	\mathcal{M}_1^\diamond			\mathcal{M}_2^\diamond			\mathcal{M}_3^\diamond		
	Worst	0.1-tail	Avg.	Worst	0.1-tail	Avg.	Worst	0.1-tail	Avg.
0.0	-69.3	-75.5	-90.8	-34.3	-58.5	-86.2	12.3	-5.0	-71.8
0.001	-44.0	-66.2	-89.4	-30.1	-54.9	-84.8	-0.7	-20.5	-73.6

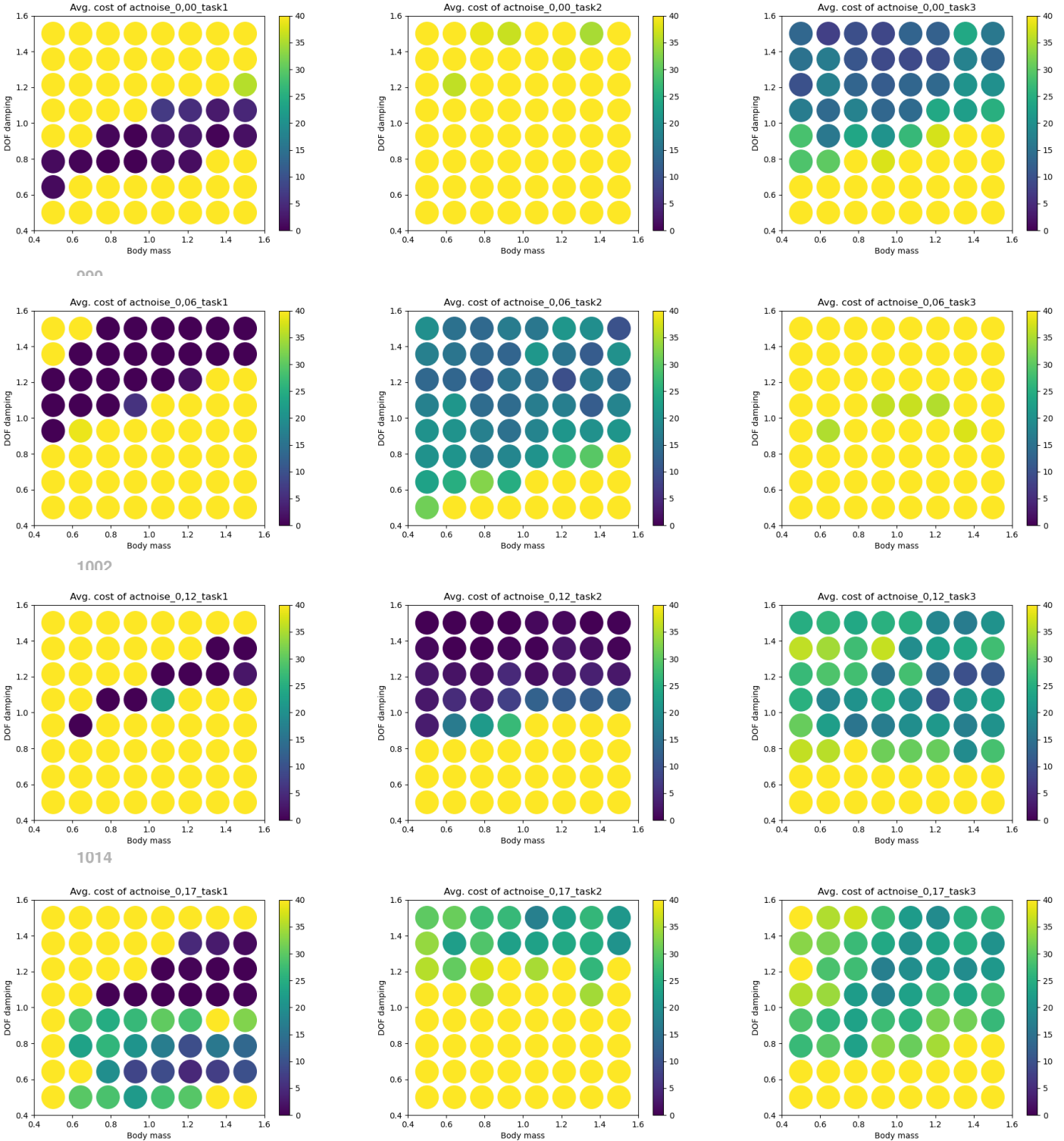
Table 9: *Deterministic students with the entropy maximizing guide.*

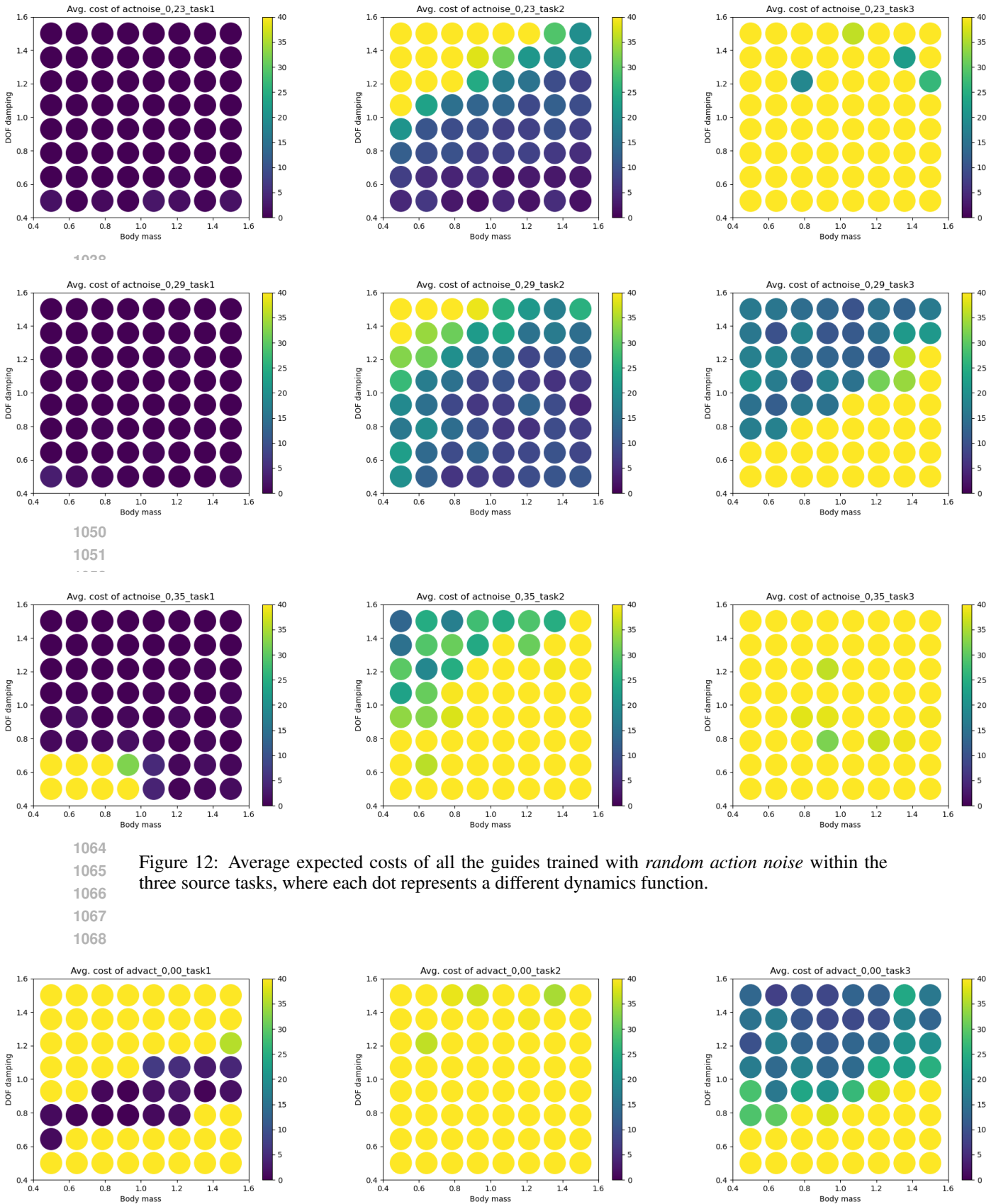
918
 919
 920
 921
 922
 923
 924
 925
 926
 927
 928
 929
 930
 931
 932
 933
 934
 935
 936
 937
 938
 939
 940
 941
 942
 943
 944
 945
 946
 947
 948
 949
 950
 951
 952
 953
 954
 955
 956
 957
 958
 959
 960
 961
 962
 963
 964
 965
 966
 967
 968
 969
 970
 971

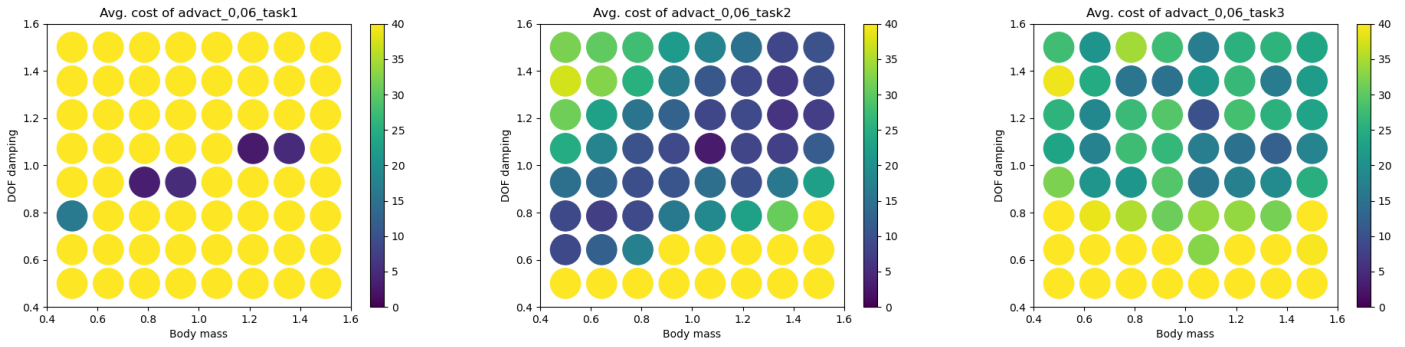
α	\mathcal{M}_1°			\mathcal{M}_2°			\mathcal{M}_3°		
	Worst	0.1-tail	Avg.	Worst	0.1-tail	Avg.	Worst	0.1-tail	Avg.
α	Worst	0.1-tail	Avg.	Worst	0.1-tail	Avg.	Worst	0.1-tail	Avg.
0.0	44.9	29.1	-46.3	80.3	45.3	-57.2	132.1	91.5	-40.1
0.001	165.2	77.6	-37.4	101.6	73.8	-51.4	137.8	108.3	-36.0

Table 10: *Nondeterministic students with the entropy maximizing guide.*

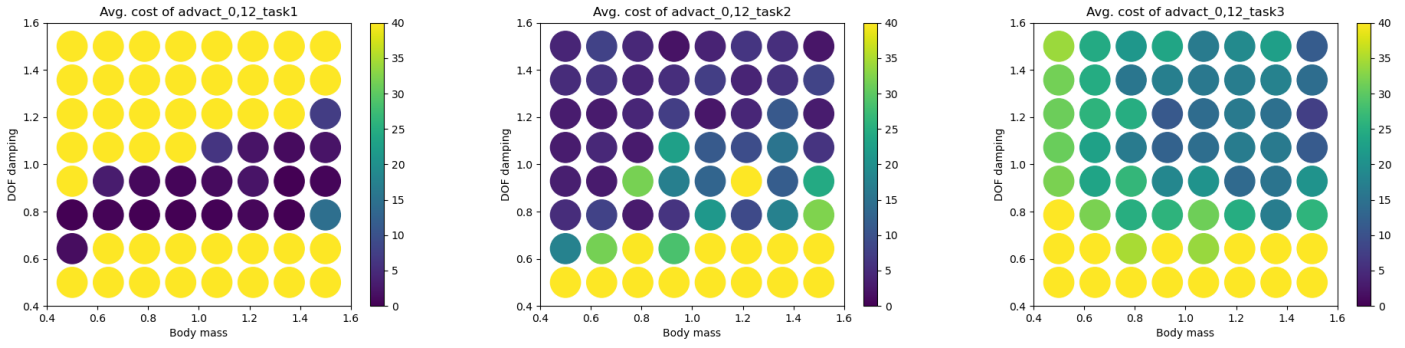
972 F ROBUSTNESS HEATMAPS FROM THE SOURCE TASK
 973
 974
 975
 976
 977



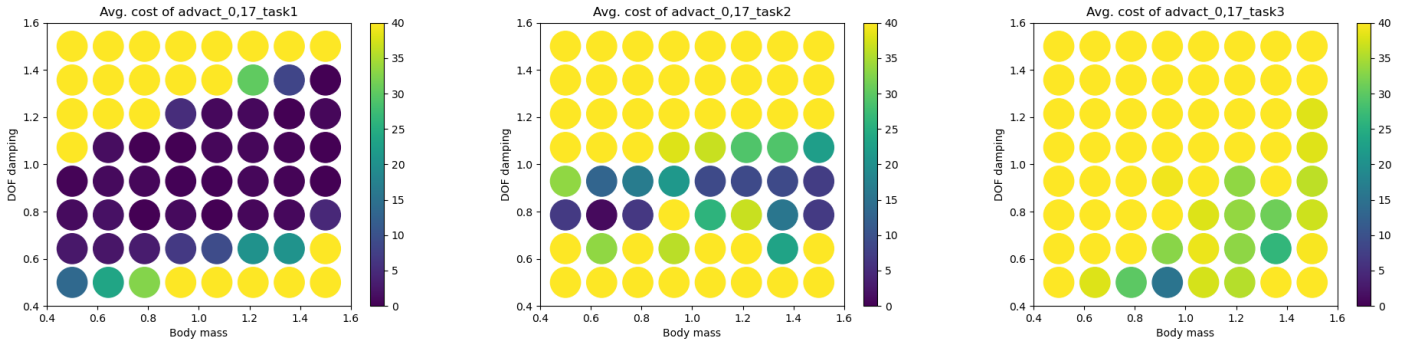




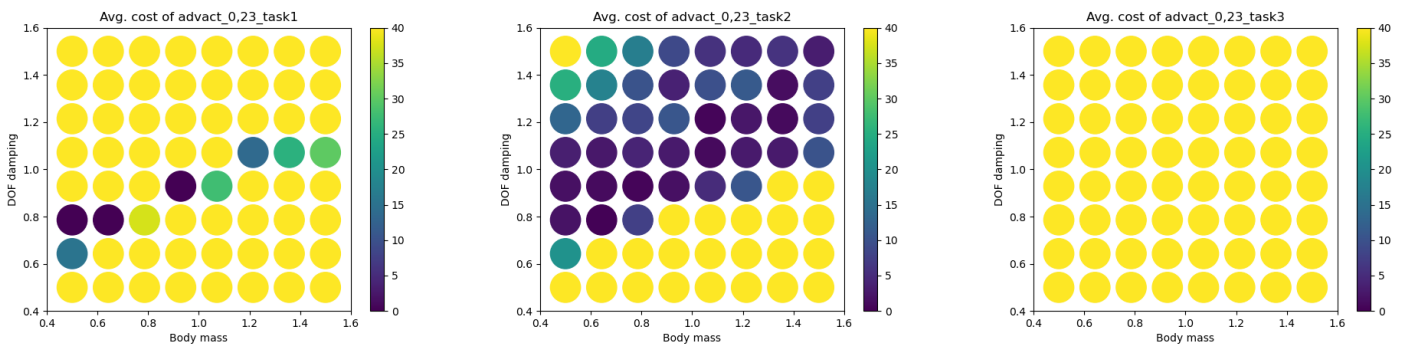
1000



1104



1116



1120

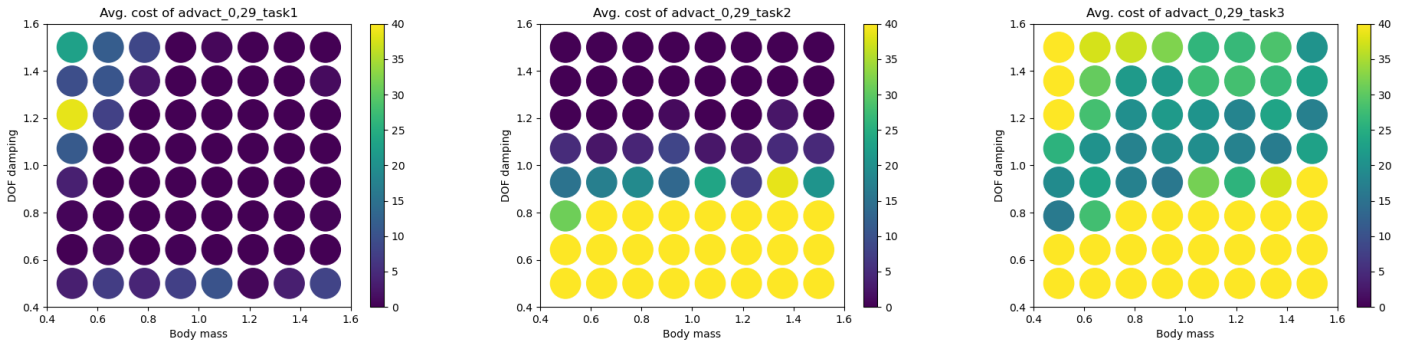
1129

1130

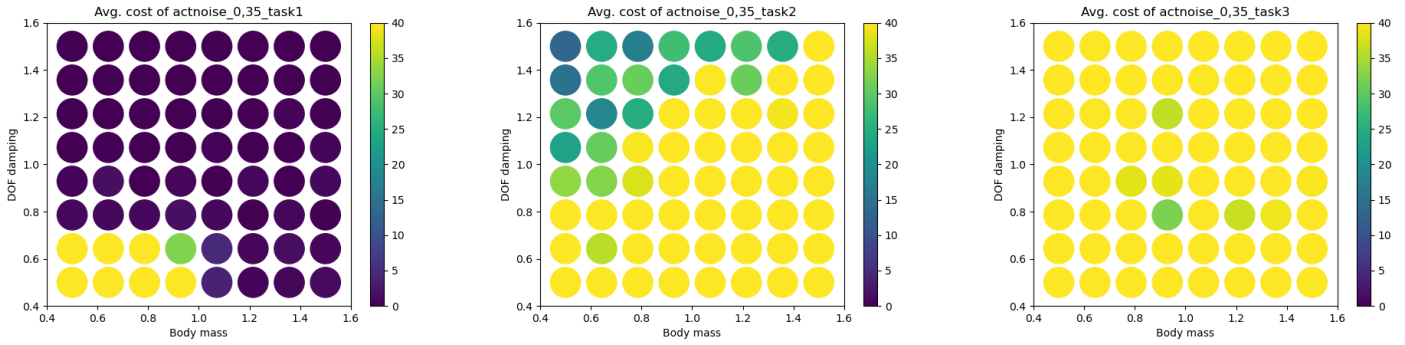
1131

1132

1133



1146



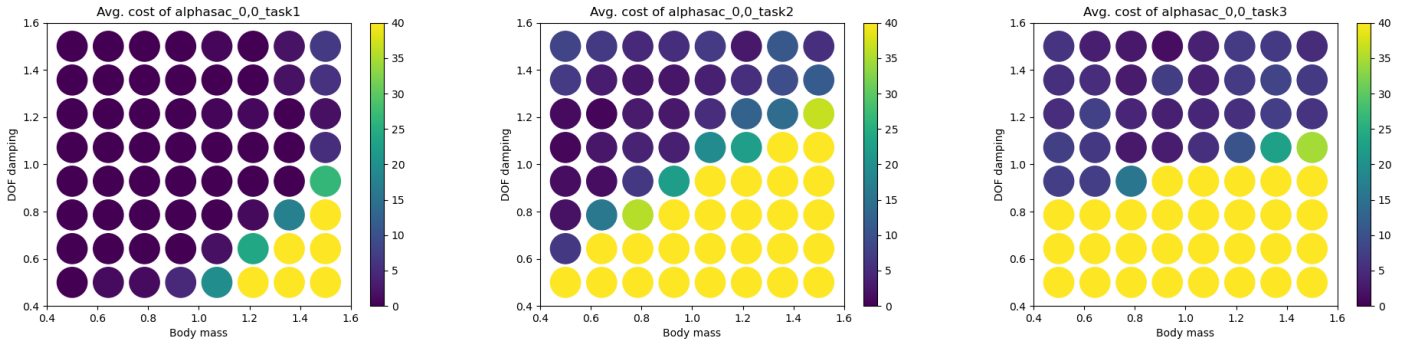
1150

1159

1160

1161

Figure 13: Average expected costs of all the guides trained with *adversarial perturbations* within the three source tasks, where each dot represents a different dynamics function.



1174

1175

1176

1177

1178

1179

1180

1181

1182

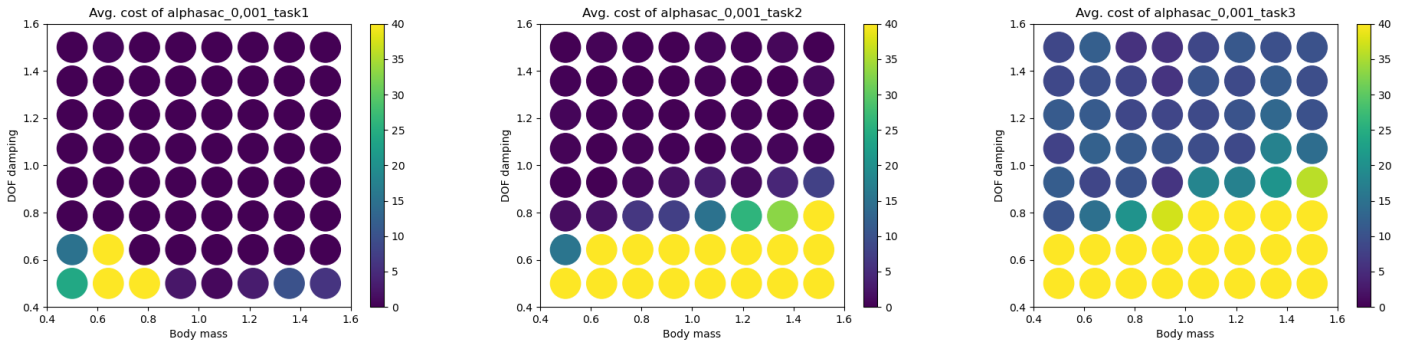
1183

1184

1185

1186

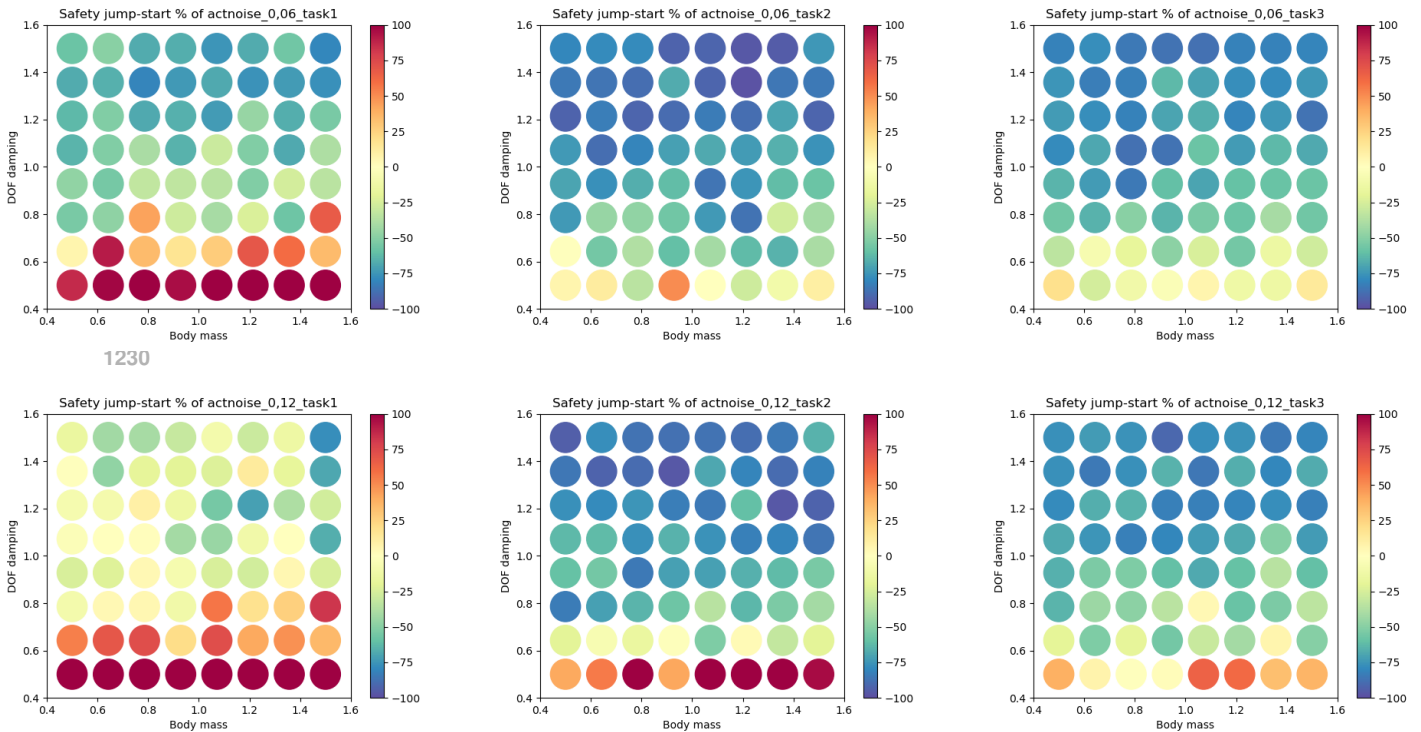
1187



1200 Figure 14: Average expected costs of all the guides trained with *entropy maximization* within the
 1201 three source tasks, where each dot represents a different dynamics function.
 1202
 1203
 1204
 1205
 1206
 1207
 1208

1209 G SAFETY JUMP-START HEATMAPS

1210
 1211
 1212
 1213
 1214
 1215 G.1 TRANSFERRING TO THE NONDETERMINISTIC STUDENT
 1216
 1217
 1218



1230

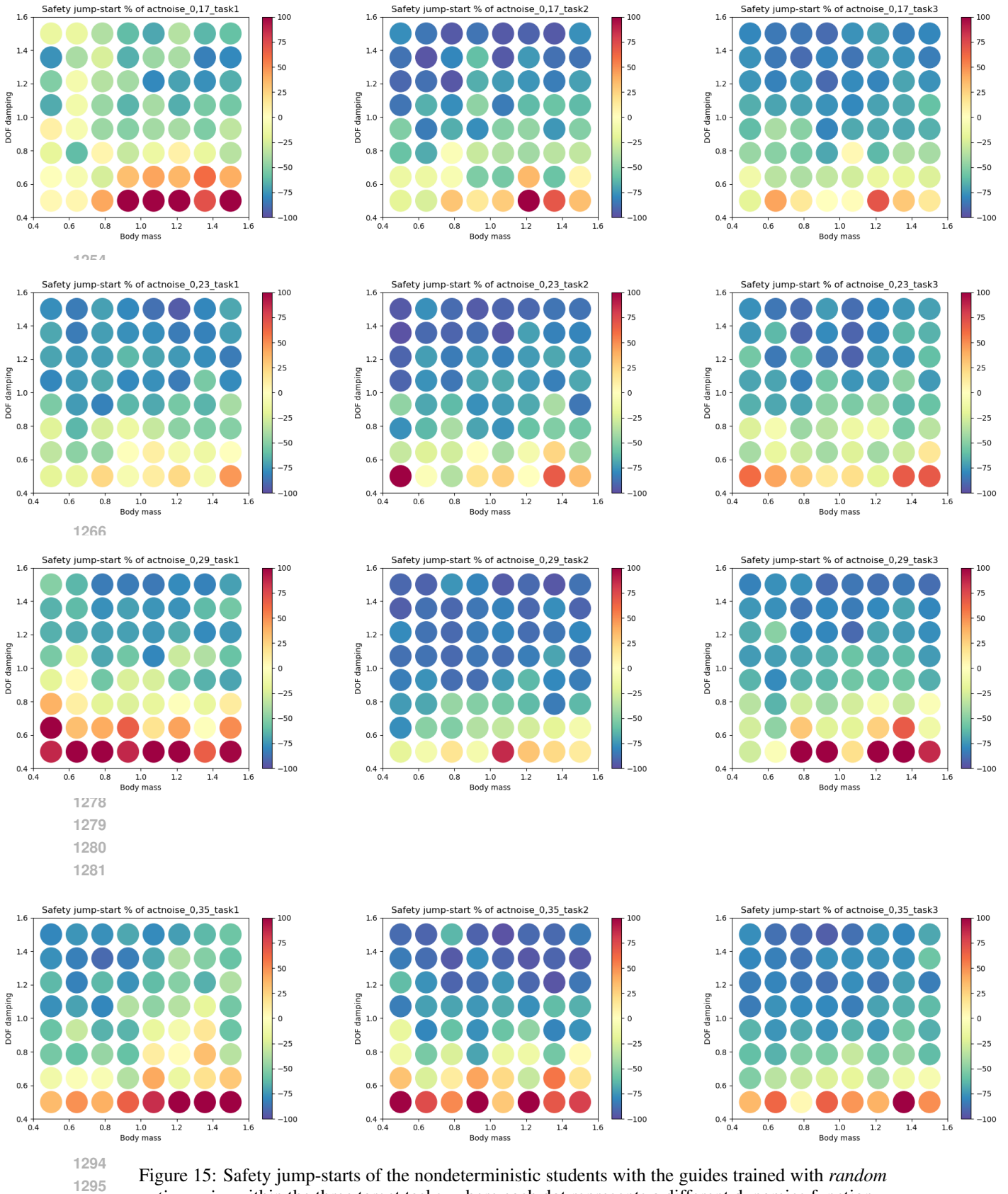
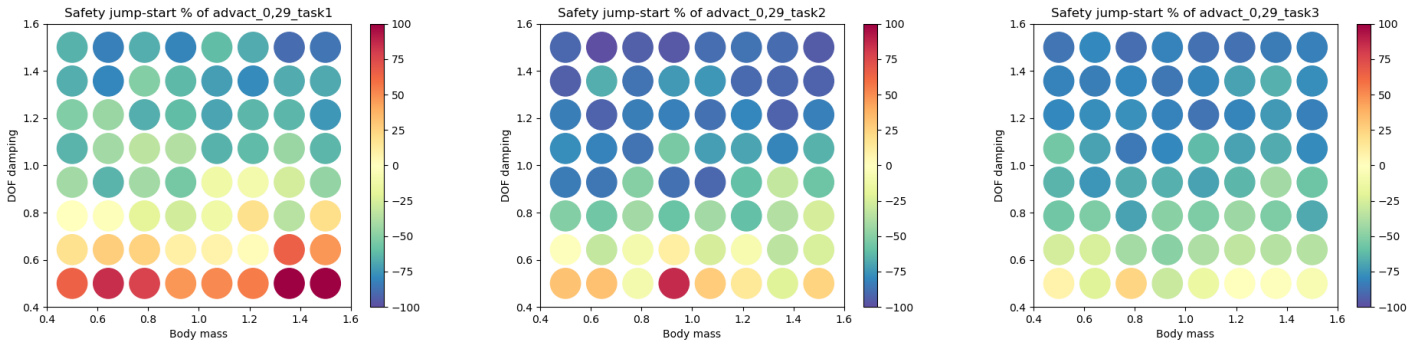
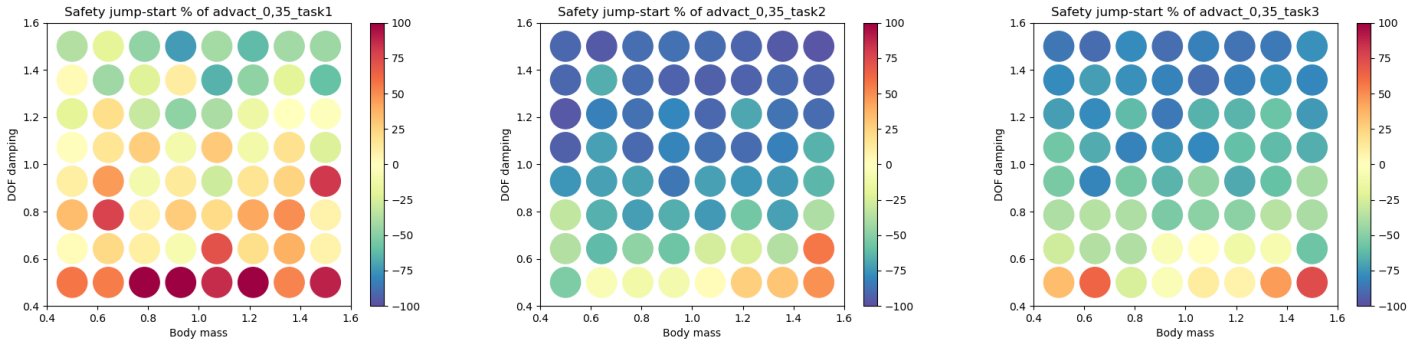


Figure 15: Safety jump-starts of the nondeterministic students with the guides trained with *random action noise* within the three target tasks, where each dot represents a different dynamics function.

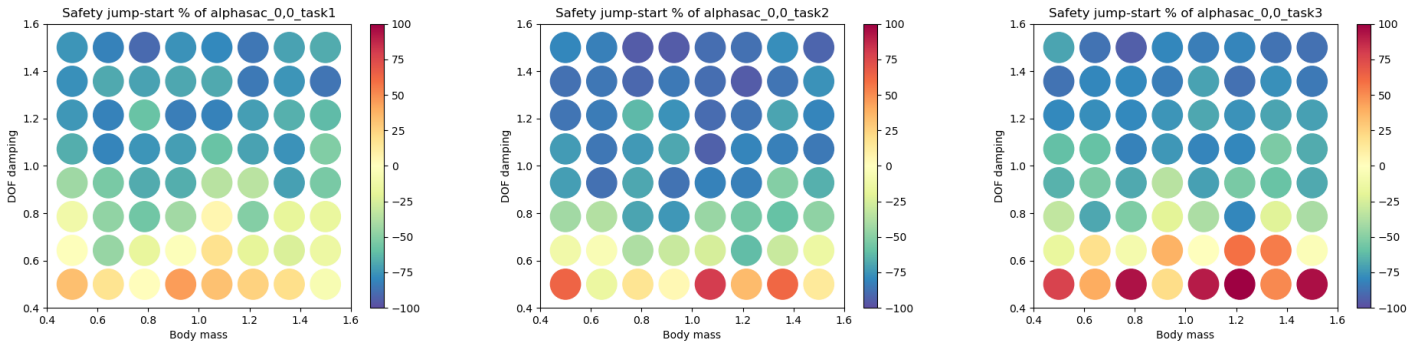


1362



1374

1375 Figure 16: Safety jump-starts of the nondeterministic students with the guides trained with *adversarial perturbations* within the three target tasks, where each dot represents a different dynamics
 1376 function.
 1377
 1378



1391

1392

1393

1394

1395

1396

1397

1398

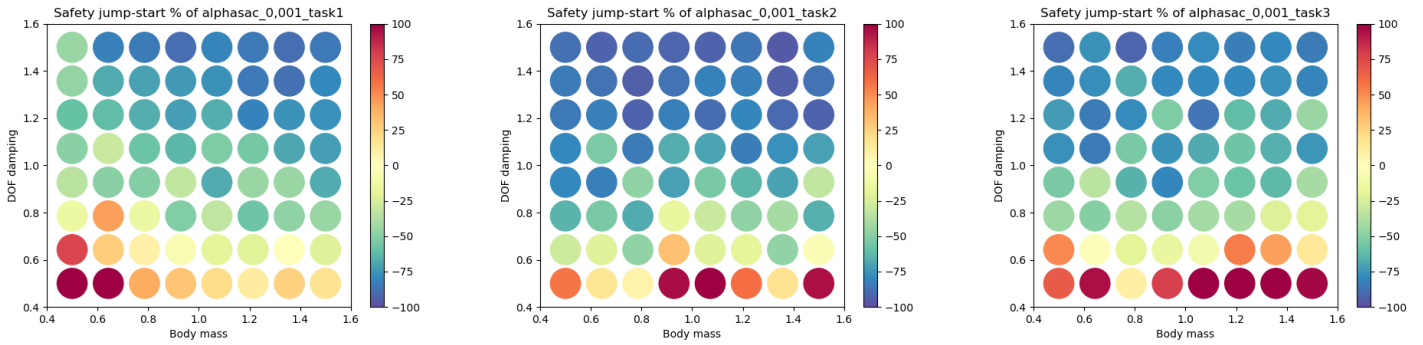
1399

1400

1401

1402

1403



1416

1417

1418

1419

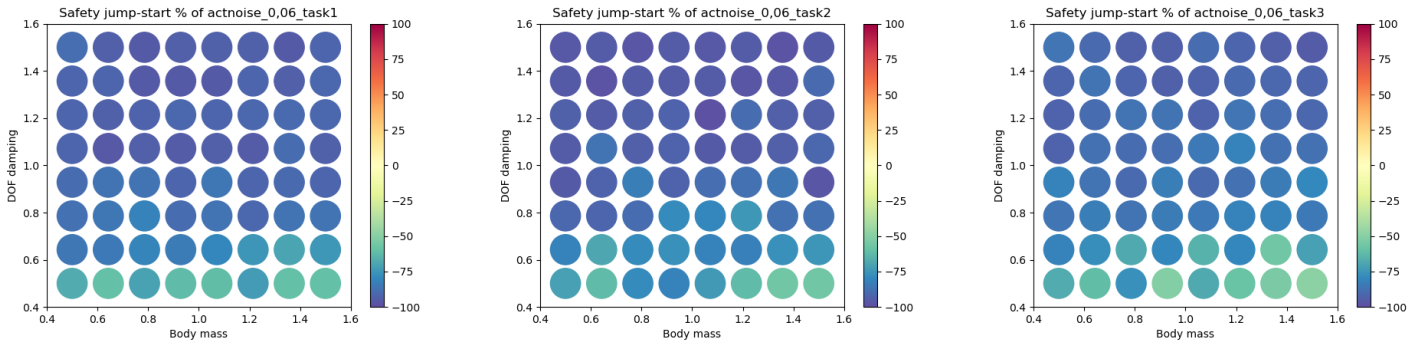
1420

1421

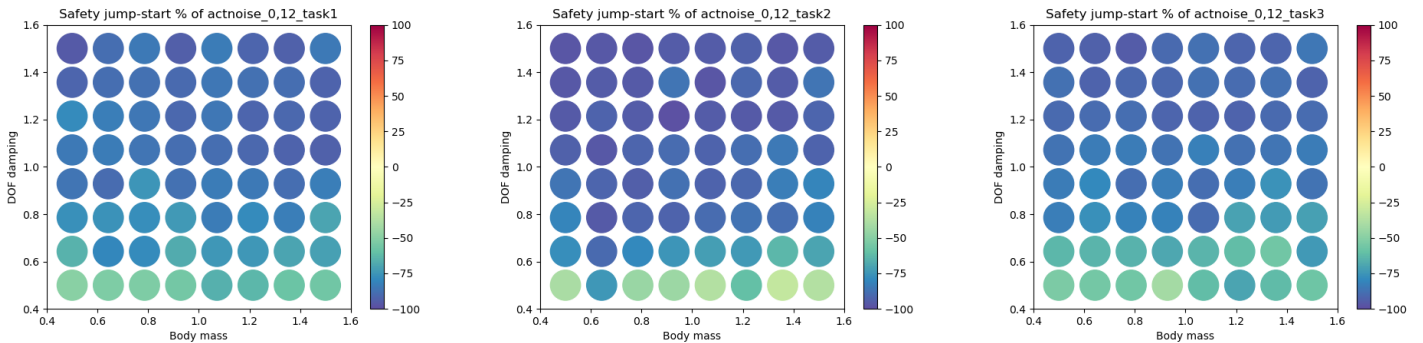
1422

Figure 17: Safety jump-starts of the nondeterministic students with the guides trained with *entropy maximization* within the three target tasks, where each dot represents a different dynamics function.

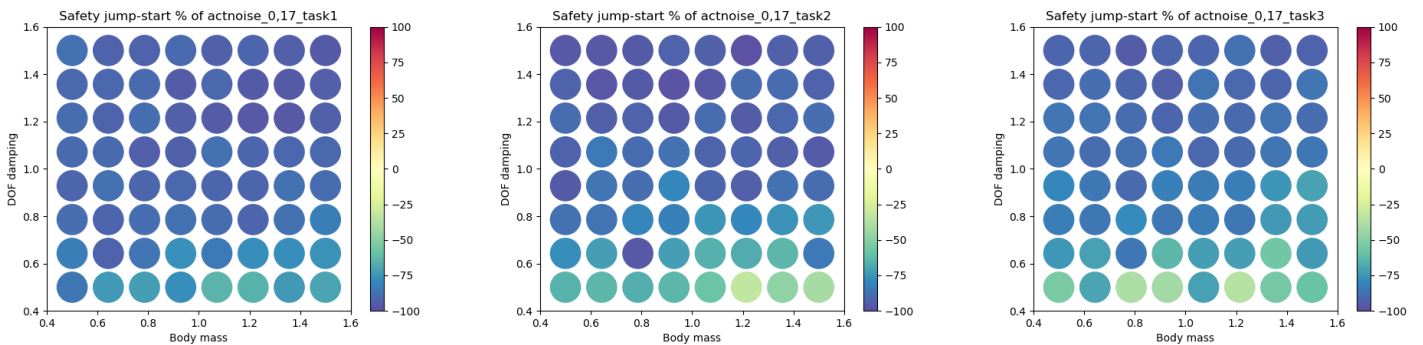
G.2 TRANSFERRING TO THE DETERMINISTIC STUDENT



1434



1446



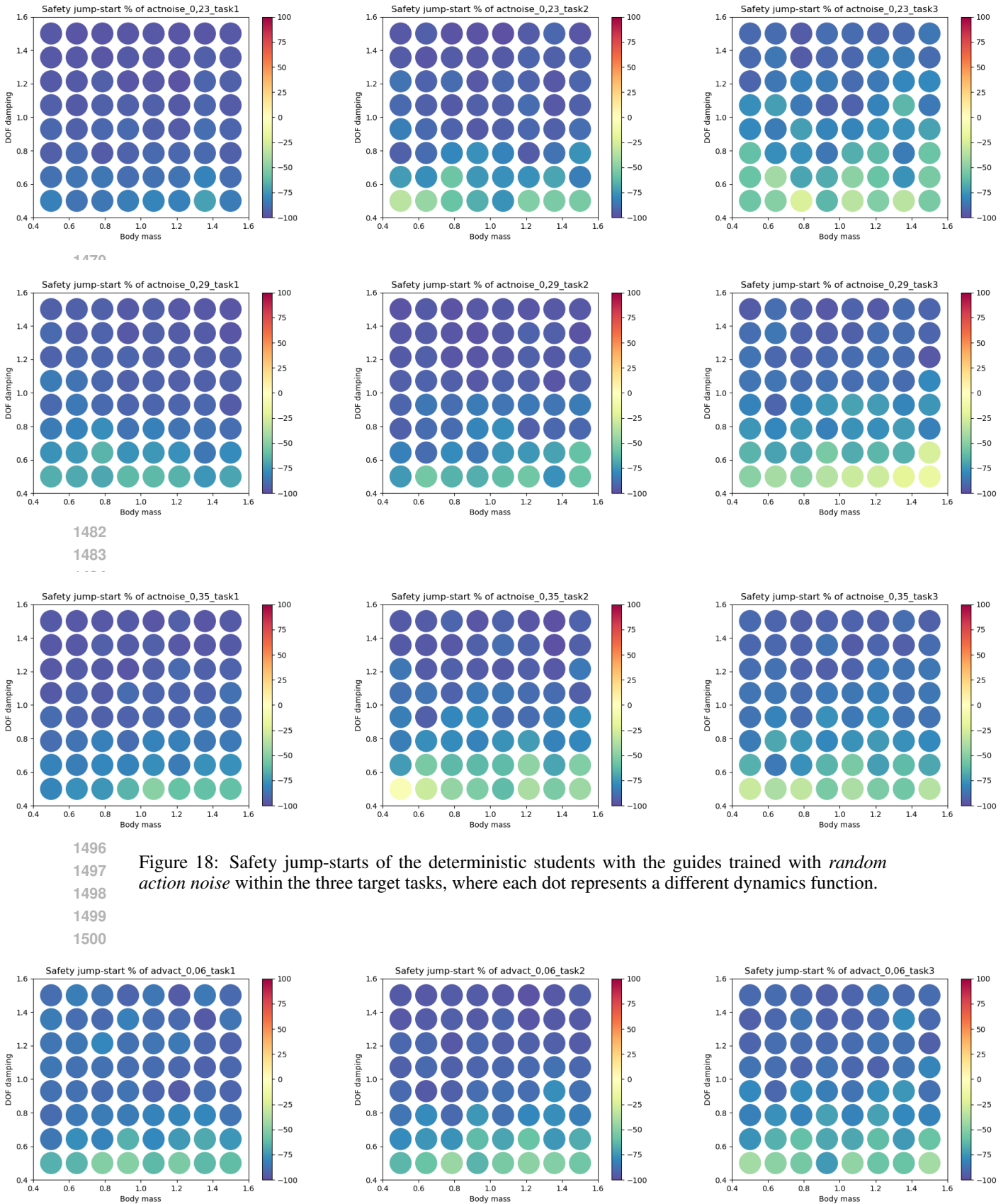
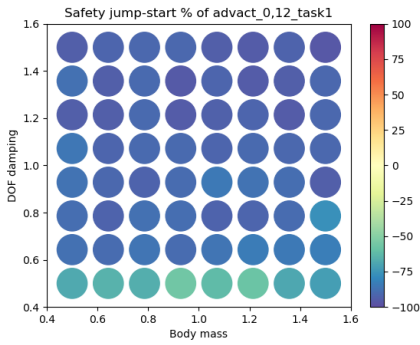
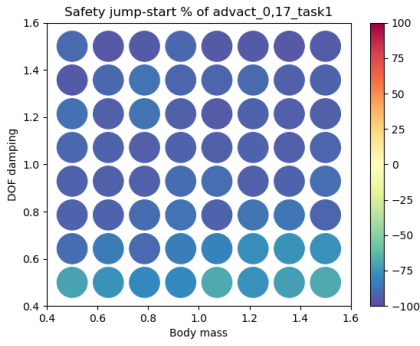
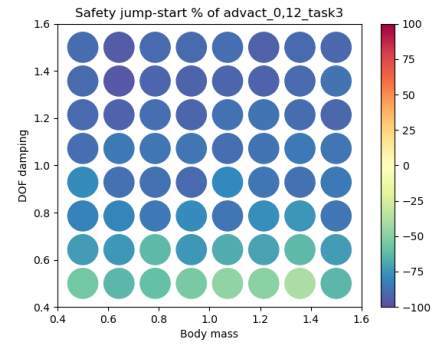
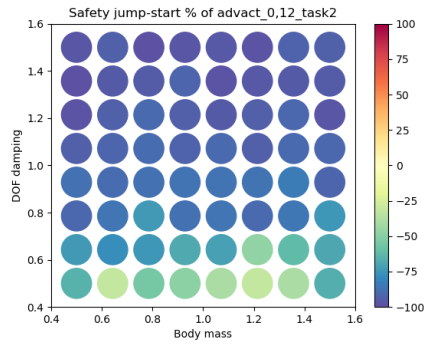


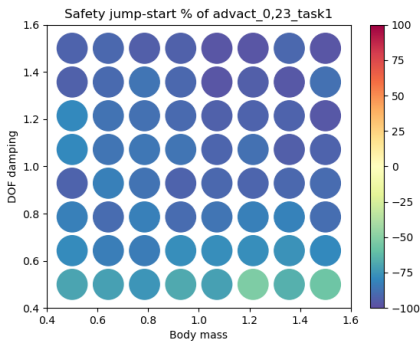
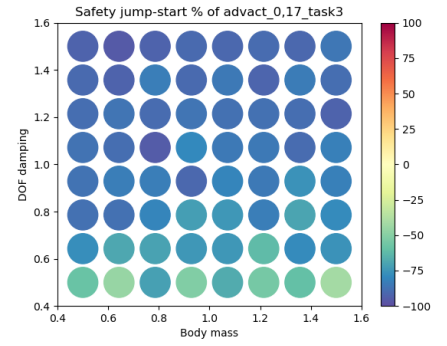
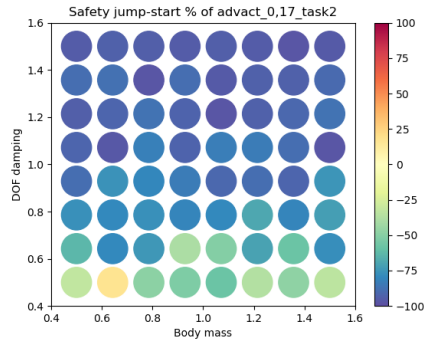
Figure 18: Safety jump-starts of the deterministic students with the guides trained with *random action noise* within the three target tasks, where each dot represents a different dynamics function.



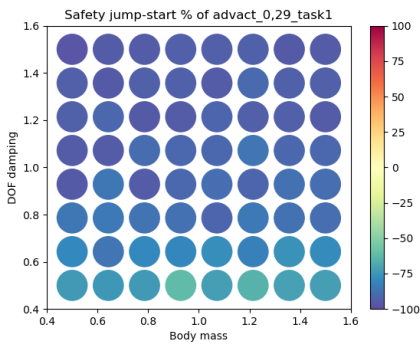
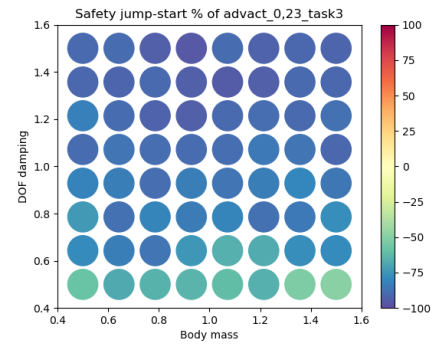
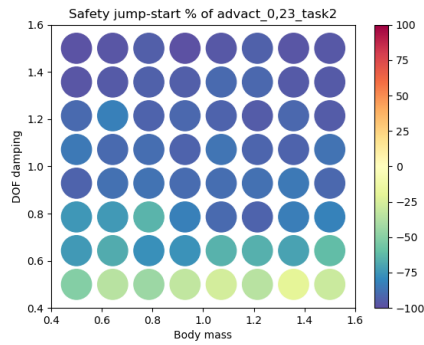
1561



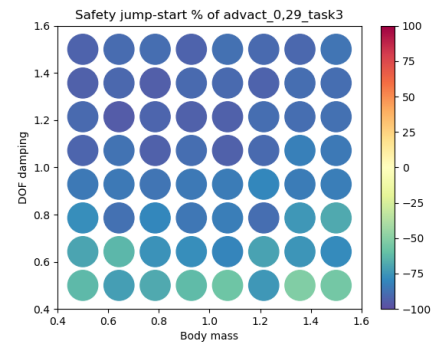
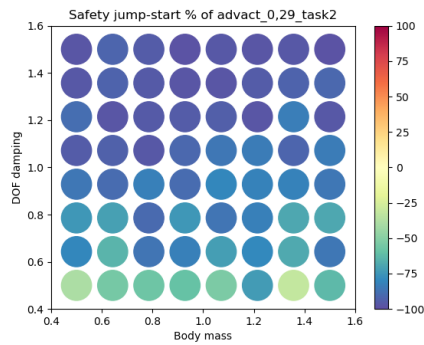
1536



1548



1500



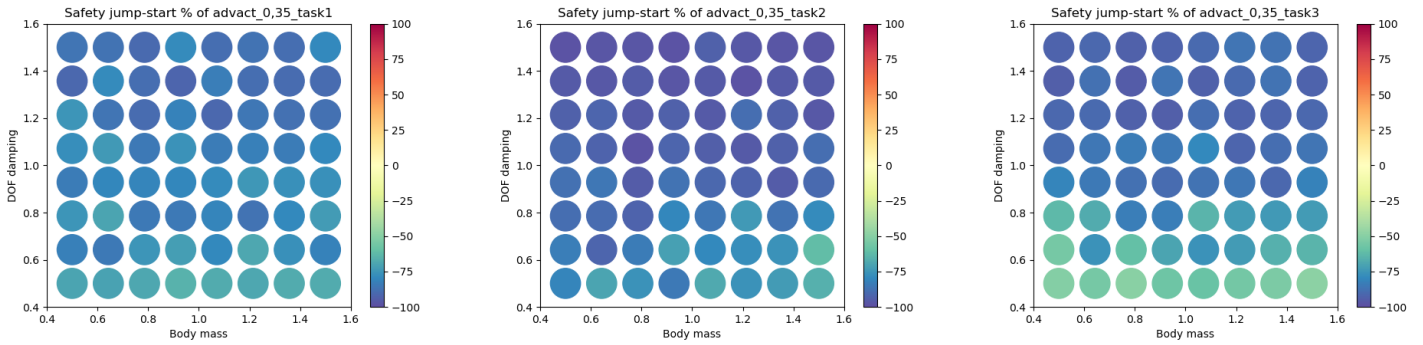
1561

1562

1563

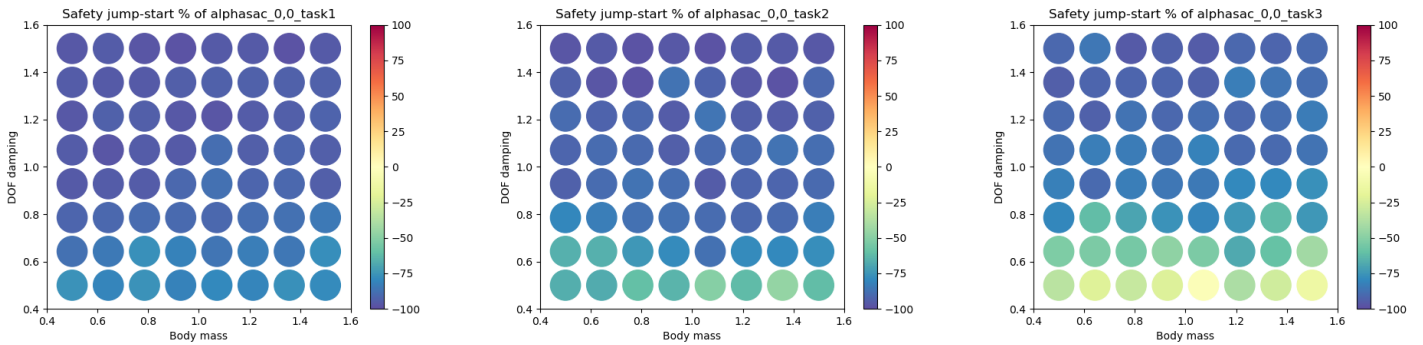
1564

1565

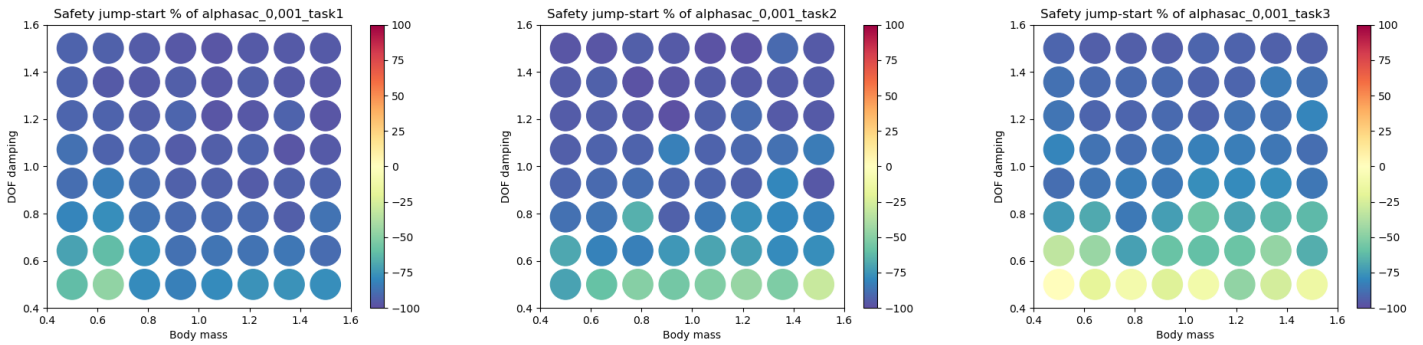


1578
1579
1580
1581

Figure 19: Safety jump-starts of the deterministic students with the guides trained with *adversarial perturbations* within the three target tasks, where each dot represents a different dynamics function.



1594



1600
1607
1608
1609
1610
1611
1612
1613
1614
1615
1616
1617
1618
1619

Figure 20: Safety jump-starts of the deterministic students with the guides trained with *entropy maximization* within the three target tasks, where each dot represents a different dynamics function.